Mechanics of Materials 189 (2024) 104874

Contents lists available at ScienceDirect

Mechanics of Materials

journal homepage: www.elsevier.com/locate/mechmat

Editor Invited Article

Mechanics of hard-magnetic soft materials: A review

Lu Lu, Jay Sim, Ruike Renee Zhao *

Department of Mechanical Engineering, Stanford University, Stanford, CA 94305, United States

ARTICLE INFO

Keywords:
Hard-magnetic soft materials
Constitutive models
Mechanical behavior
Magneto-mechanical metamaterials
Optimization design

ABSTRACT

Hard-magnetic soft materials are a class of magnetically responsive composites obtained by embedding hard-magnetic particles into a soft polymeric matrix. They have found widespread applications in shape-morphing systems, soft robotics, biomedical devices, and active metamaterials due to their ability to feature complex, untethered, reversible, and rapid deformations in response to magnetic loads. To guide the rational design of these functional applications, extensive efforts have been devoted to studying the mechanical behavior of hard-magnetic soft materials. In this paper, we review the recent progress in the mechanics of hard-magnetic soft materials. First, we introduce existing constitutive models capable of describing the coupled magneto-elastic deformations of hard-magnetic soft materials. Then, we discuss the mechanical response of structures made of hard-magnetic soft materials, including rods, beams, plates, and shells, under mechanical and magnetic loading. Subsequently, we introduce the design and behavior of magneto-mechanical metamaterials with tunable properties enabled by hard-magnetic soft materials. In addition, optimization-guided inverse design strategies for hard-magnetic soft materials to achieve predefined properties or deformations are also briefly reviewed. Finally, we provide our views on the potential future directions in the field of mechanics of hard-magnetic soft materials. We expect the current review to guide researchers to better understand different theoretical and computational frameworks of mechanics of hard-magnetic soft materials and thus aid with designing functional systems using these materials for various applications.

1. Introduction

Magnetic-responsive soft materials consisting of ferromagnetic particles and polymeric matrix have recently attracted significant research interests due to their untethered, reversible, and rapid actuation under external magnetic fields (Cui et al., 2019; Hu et al., 2018; Kim et al., 2018; Novelino et al., 2020; Wu et al., 2020b). The actuation and performance of magnetic-responsive soft materials largely depend on the magnetization of the ferromagnetic particles, the applied magnetic field, and the structure. Depending on the magnetization characteristics, ferromagnetic materials can be categorized into soft-magnetic materials and hard-magnetic materials. As shown in Fig. 1(a-i), soft-magnetic materials, such as iron and iron-nickel alloys, have low coercivity ($\mathbf{H}^c$, representing the resistance to being demagnetized), which can be readily demagnetized and remagnetized under a relatively small magnetic field. As a result, magnetic-responsive soft materials embedded with soft magnetic particles (e.g., magnetorheological elastomers and ferrogels) typically undergo simple elongation or shortening deformations by harnessing the magnetic force generated in a magnetic field. This, to some extent, limits the potential of magnetic-responsive soft materials in applications that require complex transformations.

By contrast, hard-magnetic materials, such as neodymium-iron-boron (NbFeB) and alnico, possess high coercivity ($\mathbf{H}^c$) (Fig. 1(a-i)), which makes the materials easy to maintain the remanent magnetization across a wide range of applied magnetic fields. The high remanence of saturated hard-magnetic materials allows them to maintain high residual magnetic flux density ($\mathbf{B}^r$) even in the absence of external magnetic fields. Due to these characteristics, magnetic-responsive soft materials embedded with hard-magnetic particles, referred to as hard-magnetic soft materials, can induce large magnetic body torque to create complex elastic deformation, such as bending and twisting, when the applied magnetic field is not aligned with the magnetization direction (Kim et al., 2018; Zhao et al., 2019). Such rapid and complex transformations of hard-magnetic soft materials open a new avenue for the design of functional applications like shape-morphing structures (Cui et al., 2019; Kim et al., 2018; Lum et al., 2016; Yi et al., 2022), soft robotics (Gu et al., 2020; Huang et al., 2022; Jiang et al., 2023; Ren et al., 2019; Wu et al., 2021; Xu et al., 2019; Ze et al., 2022b), flexible electronics (Deng et al.,

* Corresponding author.
E-mail address: rrzhao@stanford.edu (R.R. Zhao).

https://doi.org/10.1016/j.mechmat.2023.104874
Received 15 September 2023; Received in revised form 8 November 2023; Accepted 22 November 2023
Available online 26 November 2023

2020; Qi et al., 2021; Rahmati et al., 2023a), and active metamaterials (Chen et al., 2021a; Gu et al., 2019; Sim et al., 2023), among others. The combination of controllable remanent magnetizations of hard-magnetic soft materials and remotely tunable magnetic stimuli significantly enhance the application potential and performance of these functional designs. For example, conventional soft robots usually rely on either slow, tethered, or bulky actuators (or a combination of such). By integrating hard-magnetic soft materials, magnetic soft robots can achieve diverse functionalities across different length scales through untethered and rapid actuation under remote magnetic fields (Hu et al., 2018; Ze et al., 2022a). In addition, conventional metamaterials can only exhibit specific behavior or properties and lack tunability once they are fabricated. By incorporating hard-magnetic soft materials, the metamaterials can change their shapes and corresponding behavior or properties in response to magnetic stimuli (Montgomery et al., 2021; Wu et al., 2019, 2022).

The functional design and realization of these applications largely rely on the coupled magneto-elastic deformations of hard-magnetic soft materials. To guide the rational design of these functional applications, understanding the mechanical behavior of hard-magnetic soft materials is crucial. In recent years, extensive efforts have been devoted to studying the mechanical behavior of hard-magnetic soft materials, ranging from developing constitutive models that govern the coupled magneto-elastic deformation (Garcia-Gonzalez and Hossain, 2021; Mukherjee et al., 2021; Zhao et al., 2019), analyzing structural response (e.g., large amplitude bending and instabilities) under mechanical and magnetic loading (Rajan and Arockiarajan, 2021; Wang et al., 2020; Yan et al., 2021), exploring the design and behavior of magneto-mechanical

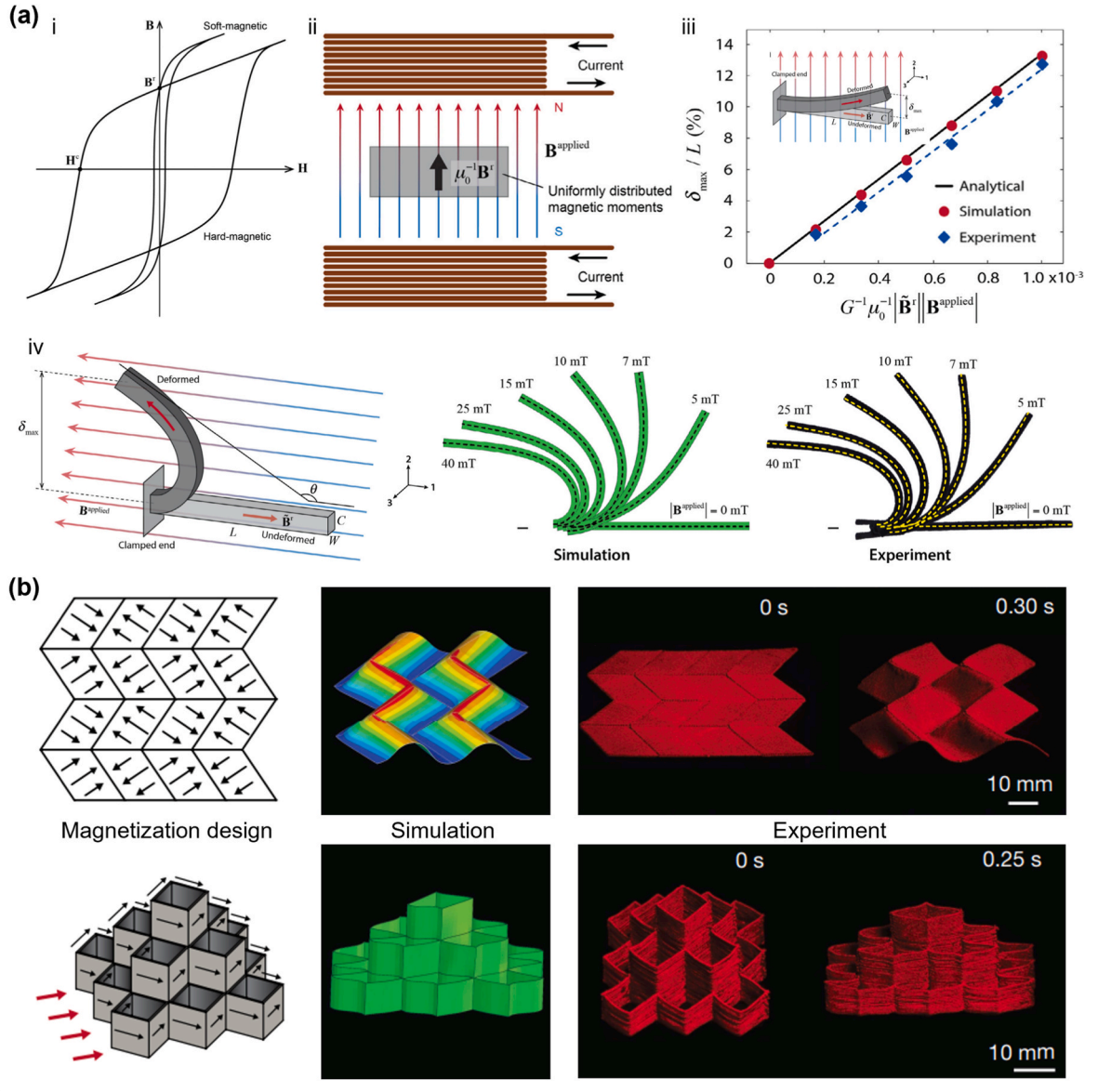

Fig. 1. Hard-magnetic soft materials. (a–i) Magnetic hysteresis loops (i.e., magnetic flux density **B** versus magnetic field **H** curves) of hard-magnetic and soft-magnetic materials. (a-ii) A hard-magnetic soft material placed in a uniform magnetic field generated by a pair of electromagnetic coils in air (or vacuum). (a-iii) Comparison of the free-end deflection of a hard-magnetic cantilever beam with small deformation under a vertical magnetic field obtained by finite element simulation, analytical solution, and experiment. (a-iv) Comparison of the deformed configuration of a hard-magnetic cantilever beam with large deformation under a horizontal magnetic field obtained by finite element simulations and experiments. (b) Comparisons of the shape-morphing of a Miura origami (top) and a pyramid-shaped thin-walled structure (bottom) under magnetic fields obtained by finite element simulations and experiments. Fig. (a) is adapted with permission from Zhao et al. (2019). Copyright 2018 by Elsevier. Fig. (b) is adapted with permission from Kim et al. (2018). Copyright 2018 by Macmillan Publishers Limited, part of Springer Nature.

metamaterials with tunable properties (Chen et al., 2021a; Ma et al., 2021), to developing optimization-guided inverse design strategies (Lum et al., 2016; Zhao and Zhang, 2022).

In this review, we focus on the recent advances in the mechanics of hard-magnetic soft materials. In Section 2, we introduce various constitutive models capable of describing the coupled magneto-elastic deformation of hard-magnetic soft materials. In Section 3, we discuss the mechanical response of structures made of hard-magnetic soft materials under external mechanical and magnetic loading, including hard-magnetic rods, beams, plates, and shells. In Section 4, we introduce the design and mechanical behavior of magneto-mechanical metamaterials with tunable properties enabled by hard-magnetic soft materials. In Section 5, we introduce optimization guided-inverse design strategies of hard-magnetic soft materials. In Section 6, we provide our insights on the future directions in the mechanics of hard-magnetic soft materials.

2. Constitutive models

To describe the coupled magneto-mechanical induced large deformation of hard-magnetic soft materials, various constitutive models have recently been developed. In this section, we introduce three typical categories of constitutive models for hard-magnetic soft materials, which consider the hyperelasticity, the dipole-dipole interactions between magnetic particles, and the viscoelasticity of the polymer matrix.

2.1. Hyperelastic constitutive model

Zhao et al. (2019) developed the first constitutive model for hard-magnetic soft materials within the framework of finite deformation theory. In the model, the hard-magnetic soft material is considered as a deformable, elastic, and homogenized continuum body, and its deformation gradient $\mathbf{F}$ is defined as

$$\mathbf{F}=\mathrm{Grad}\chi, \tag{2.1}$$

where Grad represents the gradient with respect to the position vector $\mathbf{X}$ in the reference (undeformed) configuration, and χ is the mapping of the position vector from the reference configuration to the current (deformed) configuration, i.e., $\mathbf{x}=\chi(\mathbf{X})$. The deformation Jacobian is defined as $J=\det\mathbf{F}>0$.

The magnetic field vectors in the current and reference configuration are defined as $\mathbf{H}$ and $\widetilde{\mathbf{H}}$, respectively, and the relationship between them are

$$\mathbf{H}=\mathbf{F}^{-\mathrm{T}}\widetilde{\mathbf{H}} \ \text{ or } \widetilde{\mathbf{H}}=\mathbf{F}^{\mathrm{T}}\mathbf{H}. \tag{2.2}$$

Accordingly, the magnetic flux density vector in the current and reference configurations are denoted by $\mathbf{B}$ and $\widetilde{\mathbf{B}}$, respectively, which are related by

$$\mathbf{B}=J^{-1}\mathbf{F}\widetilde{\mathbf{B}} \ \text{ or } \widetilde{\mathbf{B}}=J\mathbf{F}^{-1}\mathbf{B}. \tag{2.3}$$

Hard-magnetic soft materials have a high coercivity, allowing them to retain a high residual magnetic flux density $\mathbf{B}^{\mathrm{r}}$ over a wide range when the applied magnetic field is below the coercive field strength $\mathbf{H}^{\mathrm{c}}$. As shown in Fig. 1(a-i), it is reasonable to assume that the magnetic flux density is linearly related to the applied magnetic field within the working range, and the slope of the linear relation depends on the vacuum (or air) permeability μ_0, which gives

$$\mathbf{H}=\frac{1}{\mu_0}(\mathbf{B}-\mathbf{B}^{\mathrm{r}}). \tag{2.4}$$

For a hard-magnetic soft material under a uniform magnetic field, as shown in Fig. 1(a-ii), the magnetic potential energy, i.e., the magnetic Helmholtz free energy, per unit volume in the current configuration is equal to the work required to realign the magnetic moment $\mu_0^{-1}\mathbf{B}^{\mathrm{r}}$ along the applied magnetic field $\mathbf{B}^{\mathrm{applied}}$, which can be written as

$$W^{\mathrm{magnetic}}=-\frac{1}{\mu_0}\mathbf{B}^{\mathrm{r}}\cdot\mathbf{B}^{\mathrm{applied}}. \tag{2.5}$$

Then, the magnetic Helmholtz free energy of the hard-magnetic soft material per unit volume in the reference configuration can be obtained as

$$\widetilde{W}^{\mathrm{magnetic}}=JW^{\mathrm{magnetic}}=-\frac{1}{\mu_0}\mathbf{F}\widetilde{\mathbf{B}}^{\mathrm{r}}\cdot\mathbf{B}^{\mathrm{applied}}. \tag{2.6}$$

The elastic Helmholtz free energy $\widetilde{W}^{\mathrm{elastic}}$, namely the strain energy, per unit volume in the reference configuration is a function of the deformation gradient $\mathbf{F}$, which can be evaluated by various hyperelastic models, such as the neo-Hookean (Rivlin, 1948a), Mooney-Rivlin (Mooney, 1940; Rivlin, 1948b), Ogden (Ogden, 1972), and Arruda-Boyce (Arruda and Boyce, 1993) models.

Therefore, the total Helmholtz free energy of the hard-magnetic soft material consisting of the elastic part and the magnetic part can be expressed as

$$\widetilde{W}(\mathbf{F})=\widetilde{W}^{\mathrm{elastic}}(\mathbf{F})-\frac{1}{\mu_0}\mathbf{F}\widetilde{\mathbf{B}}^{\mathrm{r}}\cdot\mathbf{B}^{\mathrm{applied}}. \tag{2.7}$$

Note that since $\widetilde{\mathbf{B}}^{\mathrm{r}}$ and $\mathbf{B}^{\mathrm{applied}}$ are usually specified as constant values, $\widetilde{W}$ is a function of $\mathbf{F}$ only. By using Eq. (2.7), the Cauchy stress in hard-magnetic soft materials can be obtained as

$$\boldsymbol{\sigma}=\frac{1}{J}\frac{\partial\widetilde{W}(\mathbf{F})}{\partial\mathbf{F}}\mathbf{F}^{\mathrm{T}}=\frac{1}{J}\frac{\partial\widetilde{W}^{\mathrm{elastic}}(\mathbf{F})}{\partial\mathbf{F}}\mathbf{F}^{\mathrm{T}}-\frac{1}{\mu_0}\mathbf{B}^{\mathrm{applied}}\otimes\mathbf{B}^{\mathrm{r}}, \tag{2.8}$$

where the operation $\otimes$ denotes the dyadic product.

Under quasi-static conditions, the following equilibrium equation must be satisfied everywhere in the current configuration of the material:

$$\mathrm{div}\boldsymbol{\sigma}+\mathbf{f}=\mathbf{0}, \tag{2.9}$$

where div represents the divergence with respect to $\mathbf{x}$, and $\mathbf{f}$ is the body force per unit volume in the current configuration. By substituting Eq. (2.8) into Eq. (2.9) and solving the equilibrium equation, the deformation gradient $\mathbf{F}$ can be obtained, which determines the equilibrium configuration of the hard-magnetic soft material under magnetic actuation.

To validate the developed constitutive model for hard-magnetic soft materials, Zhao et al. (2019) implemented the theoretical framework into a user-element subroutine in the commercial finite element software Abaqus and compared the simulation results with analytical solutions and experiments. As shown in Fig. 1(a-iii), the free-end deflection of a hard-magnetic cantilever beam under a vertical magnetic field with small deformation, predicted by finite element simulations, shows good agreement with the theoretical predictions and experiments. Comparison of the large deformation behavior of a hard-magnetic cantilever beam under a horizontal magnetic field predicted by finite element simulations and experiments is presented in Fig. 1(a-iv). For different magnetic flux density $\mathbf{B}^{\mathrm{applied}}$, the deformed configurations of the beam obtained by the two methods are strikingly similar. The constitutive model not only accurately captures the mechanical behavior of one-dimensional (1D) slender structures, but also predicts the complex transformation of shape-morphing structures very well, such as the two-dimensional (2D) Miura origami and the three-dimensional (3D) pyramid-shaped thin-walled structure shown in Fig. 1(b) (Kim et al., 2018). Subsequently, the constitutive model has been widely used to investigate the mechanical behaviors of various structures made of hard-magnetic soft materials, which will be presented in subsequent sections.

When the applied magnetic field is not aligned with the magnetization direction, a magnetic body torque is generated to align the magnetization direction of the hard-magnetic soft material with the

magnetic field. The generated magnetic body torque per unit volume in the current configuration can be expressed as

$$\mathbf{m} = \frac{1}{\mu_0}\mathbf{B}^{\mathrm{r}} \times \mathbf{B}^{\mathrm{applied}}, \tag{2.10}$$

which creates internal stresses that enable a macroscale response of the hard-magnetic soft material. It should be stated that the magnetic Cauchy stress induced by the magnetic body torque in the material is asymmetric. As a result, the total Cauchy stress, accounting for both the magnetic and mechanical components, is also asymmetric. Therefore, the asymmetric part of the Cauchy stress and the magnetic body torque need to satisfy the conservation of angular momentum to ensure equilibrium, which gives

$$\varepsilon : \frac{\boldsymbol{\sigma} - \boldsymbol{\sigma}^{\mathrm{T}}}{2} + \mathbf{m} = \mathbf{0}, \tag{2.11}$$

where ε is the third-order permutation tensor.

In general, actuation of hard-magnetic soft materials is achieved by transferring the magnetic body torques on the embedded magnetic particles, which are generated in response to externally applied magnetic fields, to the surrounding soft matrix. The transmission efficiency of these magnetic torques to the matrix is significantly affected by the interactions between the magnetic particles and the soft matrix. To evaluate the torque transmission efficiency and understand its working mechanism, Zhang et al. (2020) studied the actuation efficiency in hard-magnetic soft materials using a micromechanics approach through representative volume element (RVE) simulations. The torque transmission efficiency is evaluated by the ratio of the total reaction torque from the matrix to the total torque generated on the magnetic particles. The torque in the matrix can be obtained from the RVE model and the torque on the particles can be acquired using Eq. (2.10). Based on the RVE simulation results, they further proposed a simple theoretical formula for the torque transmission efficiency, which is given by

$$\eta = \cos\left\{\frac{\pi}{2}\left(1 - \frac{\pi}{4}f\right)\left[1 - \exp\left(-0.165\frac{MB}{G}\right)\right]\right\}, \tag{2.12}$$

where f is the volume fraction of the magnetic particles in the material, M is the magnetization, B is magnetic flux density, and G is the shear modulus of the matrix. Their theoretical and simulation results reveal that to ensure the actuation efficiency of hard-magnetic soft materials, one needs to consider the particle volume fraction, stiffness of the matrix, and the aspect ratios of the particles.

2.2. Constitutive model with consideration of dipole-dipole interactions

Hard-magnetic soft materials are composed of hard-magnetic particles and polymeric matrices, in which the mechanical response of the materials may be influenced by the dipole-dipole interactions between the embedded magnetic particles. To take this into account, Garcia--Gonzalez and Hossain (2021) presented a constitutive model for hard-magnetic soft materials that considers the dipole-dipole interactions between magnetic particles. In their model, the total Helmholtz free energy consists of the elastic part and the magnetic part.

The magnetic Helmholtz free energy per unit volume in the reference configuration is written as

$$\Psi_{\mathrm{mag}}(\mathbf{F}, \mathbb{B}) = \Psi^{\mathrm{d-d}}_{\mathrm{mag}}(\mathbf{F}) + \psi^{z}_{\mathrm{mag}}(\mathbf{F}, \mathbb{B}), \tag{2.13}$$

where $\mathbf{F}$ is the deformation gradient and $\mathbb{B}$ is the magnetic flux density in the reference configuration. $\Psi^{\mathrm{d-d}}_{\mathrm{mag}}$ is the magnetic potential energy related to the diploe-dipole interactions, and Ψ^{z}_{mag} is the magnetic potential energy induced by the applied magnetic field. The two parts of the magnetic potential energy are calculated as

$$\psi^{\mathrm{d-d}}_{\mathrm{mag}}(\mathbf{F}) = -\frac{\mu_0}{4\pi}\frac{\varphi^2}{\gamma}\sum_{i=1}^{N}\left[\frac{3\left[\mathbf{R}\mathbb{M}\right]\cdot\left[\mathbf{F}\mathbf{R}_i^0\right]\left[\mathbf{R}\mathbb{M}\right]\cdot\left[\mathbf{F}\mathbf{R}_i^0\right]}{\left\|\mathbf{F}\mathbf{R}_i^0\right\|^5} - \frac{\left[\mathbf{R}\mathbb{M}\right]\cdot\left[\mathbf{R}\mathbb{M}\right]}{\left\|\mathbf{F}\mathbf{R}_i^0\right\|^3}\right], \tag{2.14}$$

$$\psi^{z}_{\mathrm{mag}}(\mathbf{F}, \mathbb{B}) = -\mathbf{R}\mathbb{M}\cdot\mathbf{F}\mathbb{B}, \tag{2.15}$$

in which μ_0 is the relative permeability of the vacuum, φ is the volume fraction of the magnetic particles, and γ is a parameter to account for the number of particles per representative lattice. Moreover, $\mathbf{R}_i^0$ is the dimensionless distance between magnetic particles, $\mathbb{M}$ is the magnetization in the reference configuration, and $\mathbf{R}$ is the rotation component of the deformation gradient $\mathbf{F}$, i.e., $\mathbf{R}$=$\mathbf{F}\mathbf{U}^{-1}$ with $\mathbf{U}$ being the stretch component. Eq. (2.14) shows that the influence of the dipole-dipole interactions on the overall mechanical response of the hard-magnetic soft material depends on its magnetization, the relative distance between embedded magnetic particles, as well as the volume fraction of the particles in the material. The elastic Helmholtz free energy can be defined by various hyperelastic or visco-hyperelastic models, depending on the properties of the matrix materials. Once the total Helmholtz free energy is determined, the constitutive relations can be derived.

2.3. Constitutive models with consideration of viscoelasticity

In addition to the dipole-dipole interactions, several works have also extended Zhao et al.'s model by accounting for the viscoelasticity of the polymeric matrix of hard-magnetic soft materials, including Garcia--Gonzalez (2019), Kadapa and Hossain (2022), Narayanan et al. (2023), Rambausek et al. (2022), and Stewart and Anand (2023), and so on. For example, Stewart and Anand (2023) derived a finite deformation framework for magneto-viscoelasticity of hard-magnetic soft materials, in which the overall free energy is written as

$$\Psi_{\mathrm{R}} = \Psi^{\mathrm{me,eq}}_{\mathrm{R}}(\bar{I}_1, J) + \sum_{\alpha=1}^{M}\Psi^{\mathrm{me,neq}(\alpha)}_{\mathrm{R}}\left(\overline{\mathbf{C}}, \mathbf{A}^{(\alpha)}\right) + \Psi^{\mathrm{ms}}_{\mathrm{R}}. \tag{2.16}$$

Here, $\Psi^{\mathrm{me,eq}}_{\mathrm{R}}$ is the equilibrium part of the elastic free energy which captures the elastic response of the matrix. In their model, a simple neo-Hookean free energy is employed, which is given by

$$\Psi^{\mathrm{me,eq}}_{\mathrm{R}} = \frac{1}{2}G(\bar{I}_1 - 3) + \frac{1}{2}K(J-1)^2, \tag{2.17}$$

where G and K are the shear modulus and bulk modulus, respectively, and $\bar{I}_1 = J^{-2/3}\mathrm{tr}(\mathbf{F}^{\mathrm{T}}\mathbf{F})$. $\Psi^{\mathrm{me,neq}}_{\mathrm{R}}$ is the non-equilibrium part of the elastic free energy that captures the viscous characteristic of the matrix, which is given by (Green and Tobolsky, 1946; Linder et al., 2011)

$$\Psi^{\mathrm{me,neq}(\alpha)}_{\mathrm{R}} = \frac{1}{2}G^{(\alpha)}_{\mathrm{me,neq}}\left(\left(\mathbf{A}^{(\alpha)} : \overline{\mathbf{C}} - 3\right) - \ln\left(\det\mathbf{A}^{(\alpha)}\right)\right), \tag{2.18}$$

where $G^{(\alpha)}_{\mathrm{me,neq}}$ are the non-equilibrium shear moduli, $\overline{\mathbf{C}} = J^{-2/3}\mathbf{F}^{\mathrm{T}}\mathbf{F}$, and $\mathbf{A}^{(\alpha)}$ is an internal variable to model the viscous effects. Its evolution rule is governed by a set of differential equations, as

$$\dot{\mathbf{A}}^{(\alpha)} = \frac{1}{\tau^{(\alpha)}}\left(\overline{\mathbf{C}}^{-1} - \mathbf{A}^{(\alpha)}\right) \quad \text{with initial conditions} \quad \mathbf{A}^{(\alpha)}(\mathbf{X}, t=0) = \mathbf{1}, \tag{2.19}$$

in which $\tau^{(\alpha)}$ is the relaxation time for each viscoelastic mechanism α. Moreover, $\Psi^{\mathrm{ms}}_{\mathrm{R}}$ is the magnetic free energy per unit reference volume. Here, they assume that the magnetic free energy depends on the rotation component $\mathbf{R}$ of the deformation gradient $\mathbf{F}$ ($\mathbf{F}$=$\mathbf{R}\mathbf{U}$, with $\mathbf{U}$ being the stretch component), which is written as

$$\Psi^{\mathrm{ms}}_{\mathrm{R}} = -\mathbf{R}\mathbf{m}^{\mathrm{rem}}_{\mathrm{R}}\cdot\mathbf{b}^{\mathrm{app}}, \tag{2.20}$$

where $\mathbf{m}^{\mathrm{rem}}_{\mathrm{R}}$ is the remanent magnetization in the reference configuration, and $\mathbf{b}^{\mathrm{app}}$ is the applied magnetic flux density. Based on Eqs. (2.16)-

(2.20), the first Piola-Kirchhoff stress can be obtained as

$$\begin{aligned}\mathbf{T}_{\mathrm{R}} &= J^{-2/3}G\left[\mathbf{F}-\frac{1}{3}tr(\mathbf{C})\mathbf{F}^{-\mathrm{T}}\right]+JK(J-1)\mathbf{F}^{-\mathrm{T}}\\ &+J^{-2/3}\sum_{\alpha=1}^{M}G^{(\alpha)}_{\mathrm{me,neq}}\mathbf{F}\left(\mathbf{A}^{(\alpha)}-\frac{1}{3}\left(\overline{\mathbf{C}}:\mathbf{A}^{(\alpha)}\right)\overline{\mathbf{C}}^{-1}\right)\\ &-\left(\frac{\partial\mathbf{R}}{\partial\mathbf{F}}\right)^{\mathrm{T}}\left[\mathbf{b}^{\mathrm{app}}\otimes\mathbf{m}^{\mathrm{rem}}_{\mathrm{R}}\right],\end{aligned} \tag{2.21}$$

By implementing the constitutive model in the finite-element software package FEniCS (the FEniCS codes are available online), the model can reproduce the experimental results of damped free oscillations and dynamic snap-through of hard-magnetic arcs under external stimuli (Tan et al., 2022).

Apart from the above-mentioned constitutive models, Mukherjee et al. (2021) developed an explicit dissipative model for incompressible hard-magnetic soft materials (a user-element (UEL) subroutine in ABAQUS is available online), which can capture the magnetic energy dissipation due to ferromagnetic hysteresis. Moreover, Rahmati et al. (2023b) proposed a nonlinear theoretical framework to capture the magnetoelectric effect in hard-magnetic soft materials with electrets.

3. Mechanical response of hard-magnetic soft materials

Based on the developed constitutive models, a large amount of work has focused on studying the mechanical response of structures made of hard-magnetic soft materials such as rods, beams, plates, and shells. In this section, we discuss the mechanical response of these fundamental building blocks in engineering applications under magnetic and mechanical loads. Some typical theoretical models are also briefly discussed.

3.1. Hard-magnetic slender structures

To study the mechanical behavior of hard-magnetic slender structures, diverse theoretical models have been developed. Lum et al. (2016) derived a simple beam model based on the force and torque balance, which can predict the planar motions of hard-magnetic slender structures under uniform or gradient magnetic fields. The beam is assumed to be inextensible and unshearable, meaning that the length of the beam remains unchanged, and the cross-section remains perpendicular to the centerline during deformation. With these assumptions, the governing equation of the model is given by

$$\tau_m+\int_s^L F_y ds\cos\theta-\int_s^L F_x ds\sin\theta=-\frac{EI}{A}\frac{\partial^2\theta}{\partial s^2}, \tag{3.1}$$

where E, I, L, and A are the Young's modulus, area moment of inertia, length, and cross-sectional area of the beam, respectively. θ denotes the rotation angle between the tangent direction and the reference direction of the centerline, and is a function of the arc length coordinate s and the time t. Moreover, τ_{m} is the magnetic torque, and F_x and F_y are the magnetic forces along the x and y axes, respectively, which are given by

$$\begin{aligned}\tau_m(s,t)&=[\,0\quad 0\quad 1\,]\{[\mathbf{R}(s,t)\mathbf{m}(s)]\times\mathbf{B}(t)\},\\ F_x(s,t)&=[\,1\quad 0\quad 0\,]\{[\mathbf{R}(s,t)\mathbf{m}(s)]\cdot\nabla\}\mathbf{B}(t),\\ F_y(s,t)&=[\,0\quad 1\quad 0\,]\{[\mathbf{R}(s,t)\mathbf{m}(s)]\cdot\nabla\}\mathbf{B}(t).\end{aligned} \tag{3.2}$$

Here, $\mathbf{R}$ (s, t) is the rotational matrix, $\mathbf{m}(s)$ is the magnetization profile, and $\mathbf{B}(t)$ is the magnetic field. ∇ denotes the gradient operator. Based on the developed model, the authors proposed a universal programming strategy for small-scale soft matter to achieve desired time-varying shapes, which will be further discussed in Section 5.

Later, Wang et al. (2020) reformulated this model using the principle of minimum potential energy, which was referred to as hard-magnetic elastica. Under a uniform magnetic field (i.e., $\nabla\mathbf{B}=0$), the governing equation of the hard-magnetic elastica is given by

$$\frac{EI}{A}\frac{d^2\theta}{ds^2}+MB\sin(\varphi-\theta)=0, \tag{3.3}$$

where M is the magnitude of the magnetization in the reference configuration, B is the magnitude of the magnetic field, and φ is the angle between the direction of the magnetic field and x-axis, as shown in Fig. 2(a-i). The elastica model, i.e., Eq. (3.3), was validated by comparing its theoretical predictions with finite element simulations and experimental results reported in Zhao et al. (2019), and good agreements were observed. Based on the model, the authors examined the large deformation bending behavior of hard-magnetic elastica under uniform magnetic fields with different angles φ. As shown in Fig. 2(a-ii), as the normalized magnetic field strength increases, the angular displacement at the free-end (θ_{L}) monotonically increases until it approaches φ, at which the free-end of the elastica aligns with the applied magnetic field. For the deflection of the hard-magnetic elastica at the free-end, it also monotonically increases and then becomes saturated when $\varphi\le 90^\circ$ (Fig. 2(a-iii)). However, when $\varphi>90^\circ$, the free-end deflection first increases to a peak value and then drops as the elastica bends to its final configuration. When the magnetic field is antiparallel to the x-axis, i.e., $\varphi=180^\circ$, buckling instability of the hard-magnetic elastica takes place when the magnetic field strength exceeds a critical value B_{cr}. This critical field strength can be predicted by equating the magnetic field action to a point force applied at the free end, which is given by

$$B_{\mathrm{cr}}=\frac{\pi^2 EI}{4MAL^2}. \tag{3.4}$$

Following the inextensible and unshearable assumption, several works have studied the large deformations and instabilities of hard-magnetic slender structures (Abbasi et al., 2023; Wang et al., 2021, 2022; Zhang et al., 2023b). For example, Abbasi et al. (2023) investigated the snap buckling of hard-magnetic curved beams composed of two segments with antiparallel magnetizations along the centerline, as shown in Fig. 2(b-i). The curved beam is formed by imposing an end-to-end shortening to a doubly clamped straight beam. Fig. 2(b-ii) shows that as the end-to-end shortening increases, the required magnetic field strength to trigger snapping also increases. For small values of end-to-end shortening (less than 0.1), the critical magnetic field is proportional to its square root. When the beam is under combined mechanical and magnetic loading, the mechanical load-displacement curve can be tuned by controlling the applied magnetic field (Fig. 2(b-iii)).

The elastica model assumes the structure is inextensible, meaning it does not consider the stretching deformation. Recently, Chen and Wang (2020) developed a hard-magnetic beam model considering centerline stretching. In the model, the residual magnetic flux density of the beam and the applied magnetic field are both considered to be uniform. The governing equations for the hard-magnetic beam model are written as

$$\frac{d\Phi}{d\lambda}-\frac{1}{\mu_0}\left|\mathbf{B}^{\mathrm{r}}_0\right|\left|\mathbf{B}^{\mathrm{a}}\right|\cos(\theta-\alpha)=0, \tag{3.5}$$

$$EI\frac{d^2\theta}{dx^2}-\frac{A}{\mu_0}\left|\mathbf{B}^{\mathrm{r}}_0\right|\left|\mathbf{B}^{\mathrm{a}}\right|\lambda\,\sin(\theta-\alpha)=0, \tag{3.6}$$

where Φ is the strain energy per unit reference volume, which can be evaluated by various hyperelastic models, and λ is the stretch ratio of the centerline of the beam. $\left|\mathbf{B}^{\mathrm{r}}_0\right|$ and $\left|\mathbf{B}^{\mathrm{a}}\right|$ are the residual magnetic flux density and the applied magnetic field, respectively, and μ_0 is the permeability in vacuum. Moreover, θ is the angle between the tangent direction of the centerline and the reference configuration of the beam, and α is the angle between the magnetic field and the reference configuration of the beam. E, I, and A are the Young's modulus, area moment of inertia, and cross-section area of the beam, respectively.

To verify the accuracy of the beam model, the authors compared the

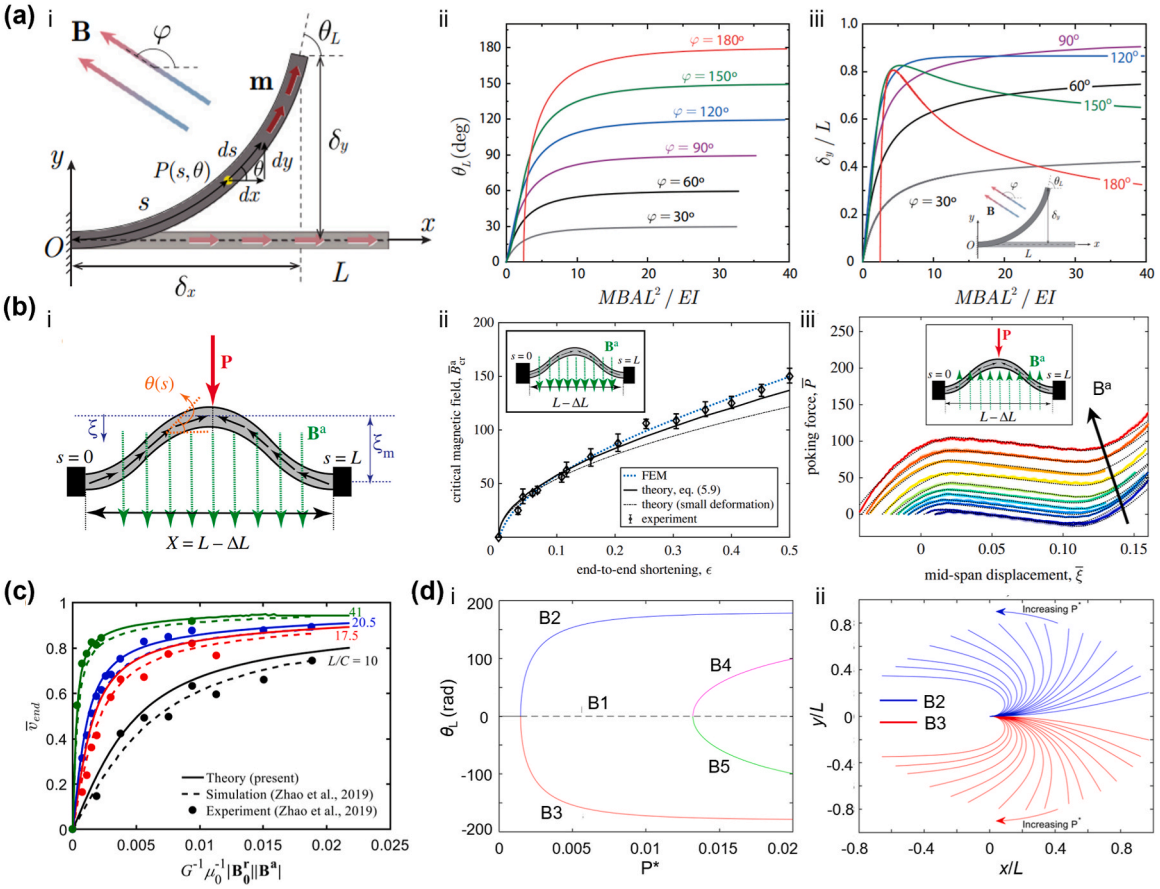

Fig. 2. Mechanical response of hard-magnetic slender structures with planar deformation. (a–i) Schematic of a hard-magnetic elastica under a uniform magnetic field. (a-ii) Free-end angular displacement and (a-iii) deflection versus normalized magnetic field strength of a hard-magnetic elastica. (b–i) Schematic of a bistable curved hard-magnetic beam under combined mechanical and magnetic loading. (b-ii) Normalized critical magnetic field of the curved beam under magnetic actuation as a function of the end-to-end shortening. (b-iii) Normalized poking force versus the mid-span displacement for the curved beam under different magnetic fields. (c) Comparison of the normalized free end deflections of hard-magnetic cantilever beams with different length-to-thickness ratio (L/C) obtained by the theoretical model, simulations, and experiments. (d–i) Free-end rotation angle as a function of the normalized magnetic flux density of a hard-magnetic cantilever beam under a uniform antiparallel magnetic field. (d-ii) Deformed configurations of the cantilever beam under a uniform antiparallel magnetic field with different magnetic flux densities. Fig. (a) is reproduced with permission from Wang et al. (2020). Copyright 2020 by Elsevier. Fig. (b) is adapted with permission from Abbasi et al. (2023). Copyright 2023. The Authors. Published by the Royal Society. Fig. (c) is reproduced with permission from Chen and Wang (2020). Copyright 2020 by ASME. Fig. (d) is adapted with permission from Dehrouyeh-Semnani (2021). Copyright 2021 by Elsevier.

free-end deflections of hard-magnetic cantilever beams predicted by their theoretical model, in which a neo-Hookean hyperelastic model is adopted to capture the stretching energy, with the free-end deflections obtained by finite element simulations and experiments in Zhao et al. (2019). As shown in Fig. 2(c), the predictions of the beam model show good agreement with the simulation and experiment results when the beams have relatively large length-to-thickness ratios (e.g., 20.5 and 41). For small length-to-thickness ratios (e.g., 10 and 17.5), the beam model overestimates the deflections due to neglecting shear deformation. In addition, the beam model shows that although the beam undergoes large deformation under the external magnetic field, the axial stretch of the centerline is small. Therefore, it is sufficient to use a linear elastic constitutive relation in the beam model, i.e., $\Phi = E\varepsilon^2/2$ with $\varepsilon = \lambda - 1$. Note that when $\lambda = 1$, Eq. (3.6) reduces to the elastica model, i.e., Eq. (3.3).

Considering small deformations of the centerline, Chen et al. (2020) derived a hard-magnetic beam model considering the effect of volume fraction of magnetic particles. In the model, the residual magnetic flux density B^{r} and the effective elastic modulus E of the beam are considered to be dependent of the particle volume fraction ψ, as (Kim et al., 2019)

$$B^{\mathrm{r}} = B^{\mathrm{r}}_{\mathrm{p}}\psi, E = E_0 \exp\left(\frac{2.5\psi}{1 - 1.35\psi}\right), \tag{3.7}$$

where $B^{\mathrm{r}}_{\mathrm{p}}$ is the magnetic flux density of the particles, and E_0 is the elastic modulus of the polymeric matrix. By using the model, the authors studied the buckling and post-buckling behaviors of hard-magnetic beams with volume fraction of the magnetic particles linearly or exponentially varying in the axial direction. Results show that the critical buckling load and the post-buckling configurations can be tuned by adjusting the volume fraction and distribution of the magnetic particles. Moreover, Dehrouyeh-Semnani (2021) studied the bifurcation behavior of hard-magnetic cantilever beams under external magnetic fields. It is revealed that when the magnetic field is antiparallel to the initial state of the beam, the beam undergoes a pitchfork bifurcation. The first two bifurcation modes are presented in Fig. 2(d-i). It is seen that the two stable branches are symmetric about the reference configuration of the beam, and the deformed configurations for different magnetic flux densities are shown in Fig. 2(d-ii).

The elastica and beam models are limited to studying planar motions of hard-magnetic slender structures. Recently, Sano et al. (2022) presented a magnetic Kirchhoff rod model that can be used to predict the mechanical response of hard-magnetic rods with natural curvatures

under geometrically nonlinear deformation in three dimensions, as shown in Fig. 3(a-i). The magnetic Kirchhoff rod equations are written as

$$\boldsymbol{F}'(s)+\boldsymbol{p}(s)+\boldsymbol{p}_{\mathrm{mag}}(s)=0, \tag{3.8}$$

$$\boldsymbol{M}'(s)+\widehat{\boldsymbol{d}}_3(s)\times\boldsymbol{F}(s)+\boldsymbol{q}(s)+\boldsymbol{q}_{\mathrm{mag}}(s)=0, \tag{3.9}$$

in which $\boldsymbol{F}(s)$ and $\boldsymbol{M}(s)$ are the internal forces and moments with s being the arc length coordinate, $\boldsymbol{p}(s)$ and $\boldsymbol{q}(s)$ are the distributed external force and torque per unit length, respectively, and $\widehat{\boldsymbol{d}}_3$ is the unit vector along the tangent direction of the centerline of the rod. Moreover, $\boldsymbol{p}_{\mathrm{mag}}(s)$ and $\boldsymbol{q}_{\mathrm{mag}}(s)$ are the distributed magnetic force and torque, respectively, which are defined as

$$\boldsymbol{p}_{\mathrm{mag}}(s)=\mathscr{M}\cdot(\nabla\boldsymbol{B}^{\mathrm{a}}),\boldsymbol{q}_{\mathrm{mag}}(s)=\mathscr{M}\times\boldsymbol{B}^{\mathrm{a}}, \tag{3.10}$$

where $\mathscr{M}$ is the magnetization density vector per unit length, and $\boldsymbol{B}^{\mathrm{a}}$ is the applied magnetic flux density vector.

By using the magnetic Kirchhoff rod model, Sano et al. (2022) studied the buckling instability of a naturally curved, twisted rod (i.e., a helix) under a constant magnetic field. For a helix with a pitch angle ψ, the critical magnetic field can be evaluated by

$$B^{\mathrm{a}*}=\left(\frac{\pi}{2L}\right)^2\frac{\mu_0}{AB^{\mathrm{r}}}\frac{EI}{\cos^2\psi+(EI/GJ)\sin^2\psi}, \tag{3.11}$$

where μ_0 is the magnetic permeability in vacuum, B^{r} is the residual magnetic flux density, A is the cross-sectional area, and L is the length of the rod. Moreover, I is the area moment of inertia, J is the torsional constant, and E and G are the Young's modulus and the shear modulus, respectively. Fig. 3(a-ii) presents the phase diagram of the buckling instability of a hard-magnetic helix. When the applied magnetic field B^{a} is smaller than $B^{\mathrm{a}}*$, the helix remains uniformly helical, as shown by the filled data in Fig. 3(a-ii), while the helix buckles when $B^{\mathrm{a}} > B^{\mathrm{a}}*$, as depicted by the open symbols. The boundary between the uniformly helical state and the buckled state corresponds to the critical buckling state, which agrees with the theoretical prediction (3.11) (dashed line in the figure) remarkably. Deformation of a hard-magnetic helix under a gradient magnetic field is further investigated based on the magnetic Kirchhoff rod model and experiments in Fig. 3(a-iii), and shows good agreement. It is shown that the magnetic field gradient is analogous to a unidirectional force. As the rescaled magnetic field gradient λ_{m} decreases, the helix contracts. Also, several other 3D hard-magnetic rod/beam models have recently been proposed (Chen et al., 2021b; Huang et al., 2023; Li et al., 2023; Sano, 2022; Wu et al., 2023; Yang et al., 2022). For example, Chen et al. (2021b) derived a 3D hard-magnetic beam model considering the coupling of stretching, bending, and twisting deformations. The model can predict the 3D large deformation behavior of initially straight beams with non-uniform magnetizations under uniform magnetic fields (Fig. 3(b-i)), such as the two examples shown in Fig. 3(b-ii) and 3(b-iii), in which the beams have an in-plane sinusoidal magnetization and an out-of-plane sinusoidal magnetization, respectively. Moreover, Huang et al. (2023) formulated a discrete magneto-elastic Kirchhoff rod model that can be used to analyze both the static and dynamic behaviors of hard-magnetic slender structures under magnetic fields.

In addition to these theoretical models, several numerical computational models have been developed to study the mechanical behavior of hard-magnetic slender structures. For example, Xing and Yong (2023) presented a finite element framework for simulating the large deformations and instabilities of visco-hyperelastic hard-magnetic soft

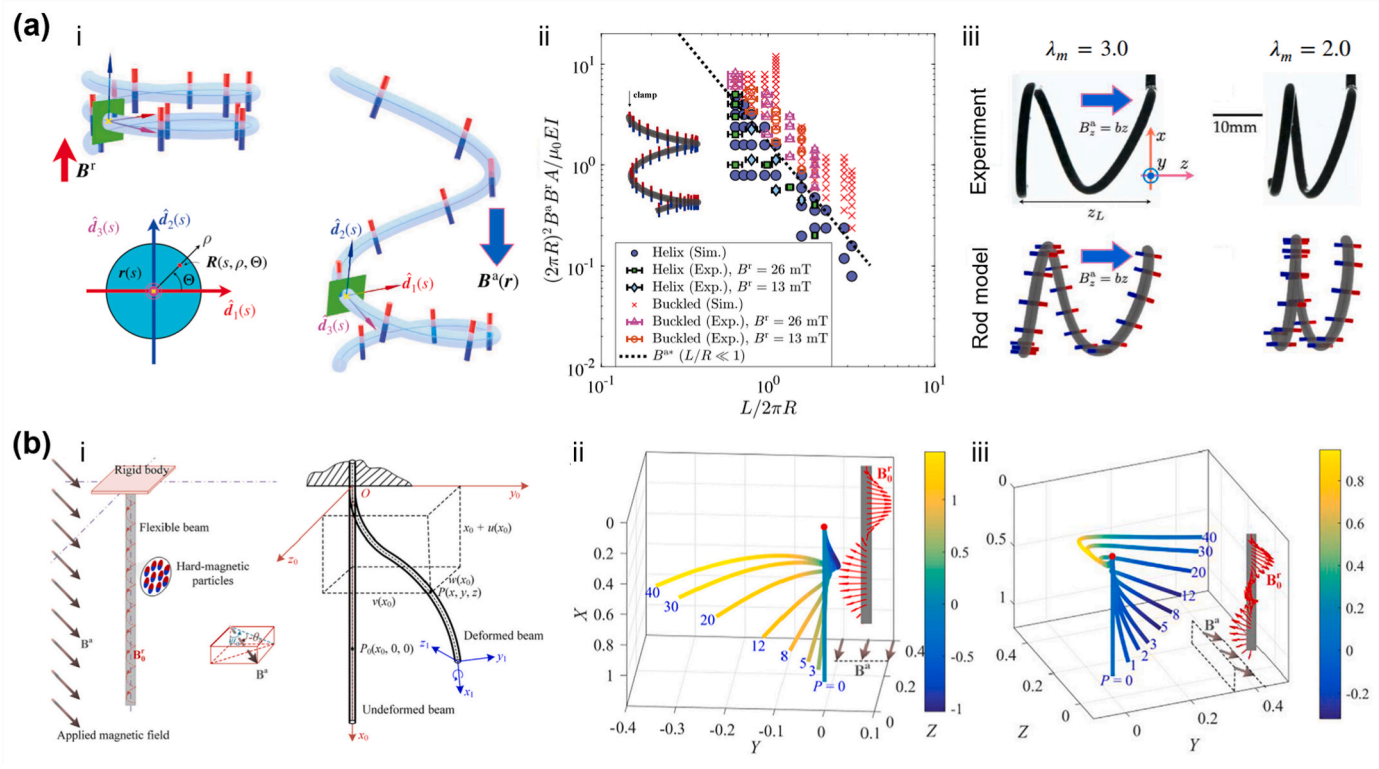

Fig. 3. Mechanical response of hard-magnetic slender structures with spatial deformation. (a–i) Schematic of a naturally curved and twisted rod under a magnetic field. (a-ii) Phase diagram for the buckling instability of a hard-magnetic helix under a magnetic field. (a-iii) Deformation of a hard-magnetic helix under a gradient magnetic field obtained by experiments and the rod model. λ_{m} denotes the rescaled magnetic field gradient. (b–i) Schematic of a hard-magnetic cantilever beam with non-uniform magnetizations under a uniform magnetic field. (b-ii) 3D deformation of a hard-magnetic beam with in-plane sinusoidal magnetization under a uniform magnetic field. (b-iii) 3D deformation of a hard-magnetic beam with out-of-plane sinusoidal magnetization under a uniform magnetic field. Fig. (a) is adapted with permission from Sano et al. (2022). Copyright 2022. The Authors. Published by Elsevier. Fig. (b) is reproduced with permission from Chen et al. (2021b). Copyright 2021 by Elsevier.

materials. Their results indicate that hard-magnetic beams show different buckling behaviors at various loading rate ranges. At moderate loading rates, delayed buckling occurs due to viscoelastic creep deformation. Ye et al. (2021) developed a lattice model for hard-magnetic soft materials by dividing the elastic energy into lattice stretching and volumetric change (the OpenFSI package for the model is available online), which can be used to investigate the large deformation of hard-magnetic beams and origami plates. By integrating with the Lattice Boltzmann method, the lattice model can predict the swimming motion of magnetic soft robots in water. Moreover, Liu et al. (2023) formulated a meshfree model for hard-magnetic soft materials based on the radial point interpolation method, which is capable of not only evaluating the bending and buckling of hard-magnetic beams but also predicting the crawling, walking, and rolling motions of hard-magnetic soft robots.

3.2. Hard-magnetic plates

Magnetic plates are also important building blocks for some engineering applications. Recently, Yan et al. (2023) derived a reduced-order model for thin hard-magnetic plates, in which the magnetization of the plate in the deformed configuration was considered to be independent of the stretching deformation. The model can predict the large deformation of hard-magnetic plates with different boundary conditions under magnetic and mechanical loading, and the predictions agree with the experiments. Chen and Tan et al. investigated the snap-through instability of a hard-magnetic flat arc formed by compressing a flat plate until it buckles (Chen et al., 2022a; Tan et al., 2022), as shown in Fig. 4(a-i). The flat arc has opposite magnetization directions in the left and right segments and is subjected to a quasi-static or dynamic magnetic field. The displacement at the middle point of the flat arc under a quasi-static magnetic field is presented in Fig. 4(a-ii). During the loading process, as the applied magnetic field increases to the threshold B^1_{cr}, the displacement snaps from point 'a' to point 'b', accompanied by the arch reversing from one equilibrium state to another. For the unloading process, the arch snaps from point 'c' to point 'd' when the applied magnetic field reaches B^2_{cr}. The two critical values of the magnetic flux density corresponding to the onset of snapping are equal in magnitude but opposite in sign, which can be estimated by (Tan et al., 2022)

$$B^1_{cr} \approx \frac{\mu_0 E\pi\xi^3}{24\sqrt{3}B^r} - \frac{\mu_0 E\pi^3\xi^3 H^2}{72\sqrt{3}B^r L^2(1-\nu^2)}, \tag{3.12}$$

where E is the Young's modulus, ν is the Poisson's ratio, L is the length, H is the thickness, $\xi = a_0\pi/L$ is the dimensionless geometric parameter with a_0 being the rise of the arc, μ_0 is the permeability in vacuum, and B^r is residual magnetic flux density. Correspondingly, the displacement at the middle point of the arc under an increasing DC pulse magnetic field is illustrated in Fig. 4(a-iii). Under the dynamic magnetic loading, the arc takes about 96 ms to reach the snapping point 'a', and then snaps to the reversed equilibrium state at point 'b' in about 48 ms. The average speed of the flat arc during the snapping process is about 120.83 mm/s, demonstrating the rapid response capability of magnetic actuation. Moreover, due to the high speed of snapping, a significant oscillation of the arc is produced by the inertia effect. In another work, Zhang and Rudykh (2022) studied the transverse elastic waves in periodic laminates made of hard-magnetic soft materials. As shown in Fig. 4(b-i), the periodic laminate consists of two isotropic incompressible alternating hard-magnetic active elastomers with different magnetizations and thicknesses. In the absence of a magnetic field, the laminate has four transverse wave band gaps (Fig. 4(b-ii)). By contrast, in the presence of a magnetic field, the band gaps are widened and shifted to higher frequencies due to the induced deformation of the magnetic excitation (Fig. 4(b-iii)). In other words, the transverse wave band gaps in hard-magnetic laminates can be actively controlled by a remotely

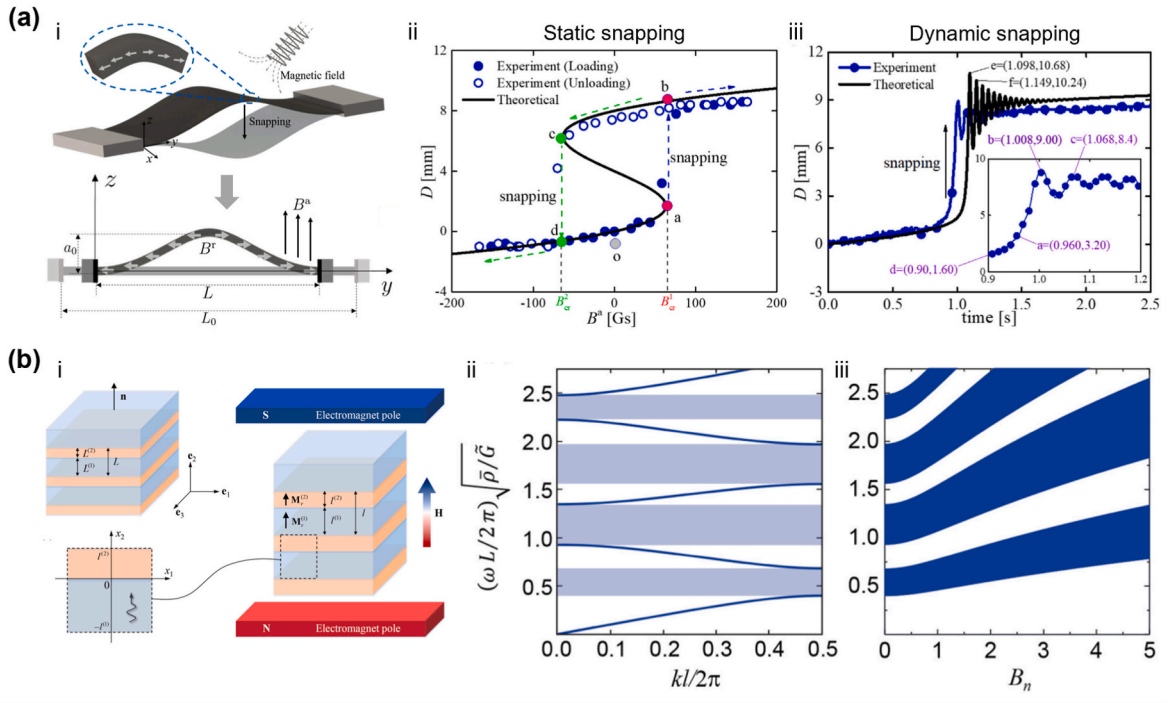

Fig. 4. Mechanical response of hard-magnetic plates. (a–i) Schematic of a hard-magnetic flat arch formed by a buckled plate. (a-ii) Snapping of the hard-magnetic flat arch under a static magnetic field. (a-iii) Snapping of the hard-magnetic flat arch under a DC pulse magnetic field. (b–i) Schematic of a hard-magnetic laminate consisting of two alternating plates with different magnetizations and thicknesses. (b-ii) Band gaps for transverse waves in hard-magnetic laminates in the absence of magnetic field. (b-iii) Band gaps for transverse waves in hard-magnetic laminates in the presence of magnetic field. Fig. (a) is adapted with permission from Tan et al. (2022). Copyright 2022 by Elsevier. Fig. (b) is reproduced with permission from Zhang and Rudykh (2022). Copyright 2022. The Authors. Published by Elsevier.

applied magnetic field. In a recent study, Alam et al. (2023) have shown that the width and position of the longitudinal wave band gaps in hard-magnetic soft laminates can also be tuned by the external magnetic field.

3.3. Hard-magnetic shells

Several works have also focused on the mechanical behavior of hard-magnetic shell structures (Chen et al., 2022b; Dadgar-Rad and Hossain, 2023; Seong et al., 2023; Stewart and Anand, 2023; Yan et al., 2021). To mention a few, Yan et al. (2021) presented a robust mechanism to dynamically tune the buckling strength of shells by exploiting the coupled magneto-mechanical deformation in hard-magnetic soft materials. The considered hemispherical shell is made of hard-magnetic soft material and its magnetization direction is perpendicular to its equatorial plane. It is shown from Fig. 5(a-i) that when applying a magnetic field in the same direction as the magnetization, the critical buckling pressure of the shell increases and the pressure gradually drops at the onset of buckling. By contrast, when the applied magnetic field is opposite to the magnetization of the shell, the critical buckling pressure decreases, and the pressure drop is more abrupt. This indicates that the buckling strength of a hard-magnetic shell can be tuned by the external magnetic field on demand. Furthermore, the knockdown factor (i.e., the ratio of the critical buckling pressure of an imperfect shell with respect to that of its perfect counterpart) of a hard-magnetic shell with geometric defect can also be adjusted by the applied magnetic field. To demonstrate this, Yan et al. (2021) fabricated a series of hard-magnetic shells with axisymmetric 2D defects of varying amplitudes at their poles (defect profiles are depicted in Fig. 5(a-ii)) and tested their knockdown factors. As shown in Fig. 5(a-iii), when the magnetic field is aligned with the magnetization direction, the knockdown factors of the hard-magnetic shells increase as the applied magnetic flux density increases for different defect amplitudes, and the increment can be up to about 30% within the accessible magnetic field compared to the no-field case. Stewart and Anand (2023) formulated a magneto-viscoelastic constitutive model for hard-magnetic soft materials and studied the snap-through eversion of a hemispherical shell induced by magnetic actuation. The shell has a uniform remanent magnetization in the $\mathbf{e}_2$-direction. As shown in Fig. 5(b-i), when applying a 200 mT magnetic field opposite to the $\mathbf{e}_2$-direction but with a slight 1° misalignment, the hemispherical shell everts itself in 0.1 s by harnessing the snap-through instability. Moreover, the eversion is reversible. When applying an 80 mT magnetic field aligned with the $\mathbf{e}_2$-direction but with a slight 1° misalignment, the hemispherical shell reverts to its initial configuration, as illustrated in Fig. 5(b-ii). Variations of the applied magnetic flux density and the induced displacement at top of the shell (red point)

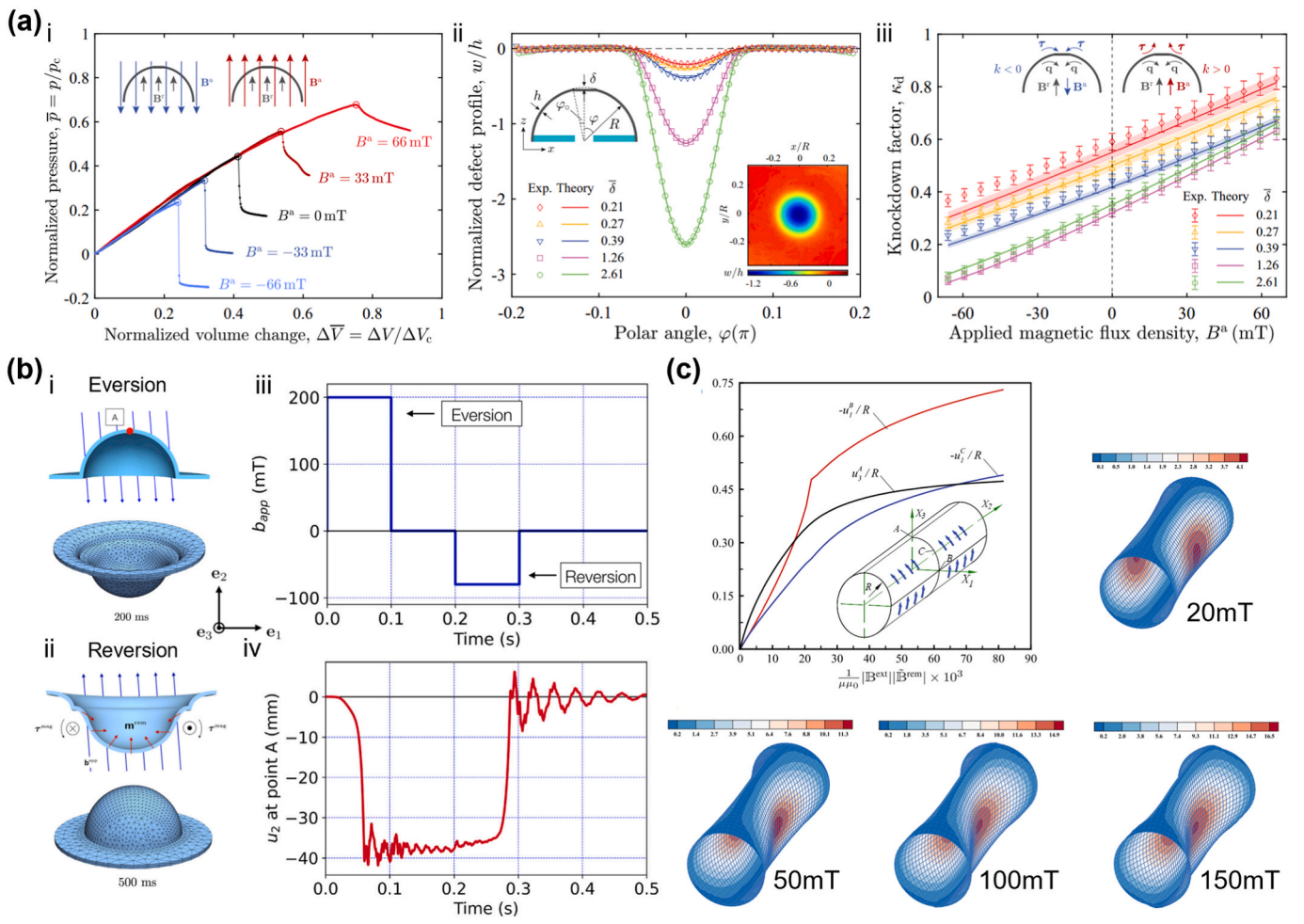

Fig. 5. Mechanical response of hard-magnetic shells. (a–i) Tunable buckling strength of a hard-magnetic shell under combined pressure and magnetic loading. (a-ii) Axisymmetric 2D defect profiles for hard-magnetic shells. (a-iii) Tunable knockdown factors of hard-magnetic shells with different defect geometries. (b) Dynamic snap-through eversion and reversion of a hard-magnetic hemispherical shell under a uniform magnetic field. (c) Elastic deformation of a hard-magnetic cylindrical shell under a uniform magnetic field. Fig. (a) is adapted with permission from Yan et al. (2021). Copyright 2021. The Authors. Published by Springer Nature. Fig. (b) is adapted with permission from Stewart and Anand (2023). Copyright 2023 by Elsevier. Fig. (c) is reproduced with permission from Dadgar-Rad and Hossain (2023). Copyright 2022. The Authors. Published by John Wiley & Sons Ltd.

during eversion and reversion are shown in Fig. 5(b-iii) and 5(b-iv), respectively. It is seen that the hemispherical shell undergoes an obvious oscillation during the dynamic snap-through instability. In another work, Dadgar-Rad and Hossain (2023) developed a 10-parameter micropolar shell model to simulate the finite elastic deformation of thin hard-magnetic soft materials. Using the micropolar shell model, they studied the elastic response of a doubly clamped hard-magnetic cylindrical shell under magnetic loading. As shown in Fig. 5(c), the remnant magnetic flux density of the cylindrical shell is tangent to its surface and has a positive component along the X_3 axis. When subjected to a magnetic field in the X_3 direction, as the magnetic flux density increases, the displacement components at points A, B, and C on the surface of the shell gradually increase, and the contraction deformation of the shell becomes prominent.

4. Magneto-mechanical metamaterials

Mechanical metamaterials are a class of architected structures often consisting of specifically designed periodic building blocks (Bertoldi et al., 2017; Yu et al., 2018), which have attracted a great deal of attention in recent years due to their unique properties and functionalities that differ from conventional materials. These metamaterials can have negative Poisson's ratio (Lakes, 1987; Saxena et al., 2016), high stiffness-to-weight ratio (Zheng et al., 2014), compression-torsion coupled deformation (Frenzel et al., 2017), and multistability (Zhang et al., 2021). However, conventional mechanical metamaterials can only exhibit specific behavior once they are fabricated, resulting in a lack of tunability. Hard-magnetic soft materials enable fast, untethered, and reversible actuation by the application of a remotely applied magnetic field (Kim et al., 2018), which provide an ideal platform for the design of

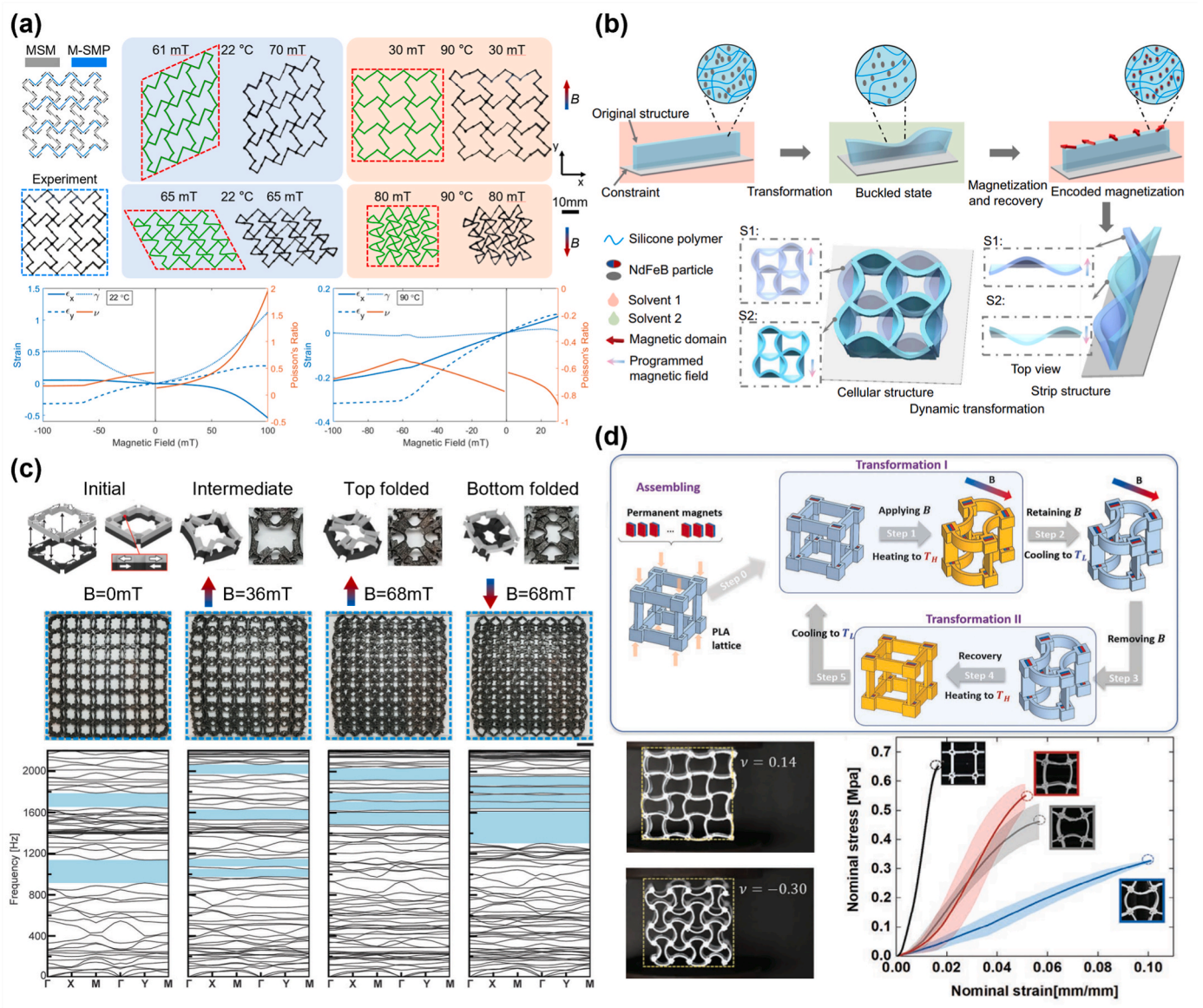

Fig. 6. Magneto-mechanical metamaterials enabled by shape transformation. (a) Magneto-mechanical metamaterials with tunable deformation mode and Poisson's ratio. (b) Magneto-elastomers with dynamic shape transformation capacity that can manipulate fluid transport. (c) Magneto-mechanical bilayer metamaterial that can maintain its overall area while tuning the acoustic/elastic bandgaps. (d) Magneto-thermomechanical metamaterial with tunable stiffness and Poisson's ratio, and shape-locking capacity. Fig. (a) is adapted with permission from Ma et al. (2021). Copyright 2020 by American Chemical Society. Fig. (b) is reproduced with permission from Xia et al. (2022). Copyright 2022. The Authors. Published by Springer Nature. Fig. (c) is adapted with permission from Sim et al. (2023). Copyright 2023 by Wiley-VCH GmbH. Fig. (d) is adapted with permission from Zou et al. (2023). Copyright 2022 by Wiley-VCH GmbH.

active mechanical metamaterials with tunable properties or functionalities. Recently, a variety of active mechanical metamaterials have been developed based on the hard-magnetic soft materials.

4.1. Shape transformation enabled magneto-mechanical metamaterials

Shape transformation is one commonly used strategy to achieve the tunable properties or behavior of magneto-mechanical metamaterials. Wu et al. (2019) developed an active metamaterial by employing an asymmetric joint design using hard-magnetic soft materials. The asymmetric joint has a bending mode based on elastic deformation and a folding mode based on rigid body rotation under opposite-direction magnetic fields. By regulating the magnetic field, the metamaterial can change its shape and thus tune its stiffness. Based on the magnetic-responsive asymmetric joint design, Montgomery et al. (2021) presented a magneto-mechanical metamaterial whose mechanical properties (e.g., Poisson's ratio and stiffness) and acoustic/elastic bandgaps can be actively controlled in a wide range by coupled magnetic actuation and mechanical forces. Recently, Ma et al. (2021) fabricated a magneto-mechanical metamaterial with multiple unique shape configurations by integrating magnetic soft materials (MSM) with magnetic shape memory polymers (M-SMP). As shown in Fig. 6(a), at room temperature (22 °C), the metamaterial shows a shear deformation mode because only the MSM component can deform due to the high stiffness of the M-SMP part at low temperature. By contrast, at a high temperature (90 °C), both materials deform simultaneously, and the metamaterial shows a biaxial deformation mode. By altering the magnetic field, the strain and Poisson's ratio at the two deformation modes can be programmed. In another work, Alapan et al. (2020) presented an auxetic metamaterial using hard-magnetic soft materials with reprogrammable magnetizations. The metamaterial shows a tunable negative Poisson's ratio under a given magnetic field, while exhibiting a tunable positive Poisson's ratio by reprogramming the magnetization through heating. In addition to programming mechanical properties, magneto-mechanical metamaterials can also be designed to tune fluidic properties in water. Xia et al. (2022) fabricated a metamaterial using silicone elastomers doped with NdFeB particles where the shape-morphing behavior can be actuated by solvent and magnetic stimuli. As shown in Fig. 6(b), when immersed in the organic solvent, the magneto-elastomer deforms into a wave shape. When subjected to a time-varying magnetic field, the positions of the peaks and troughs change with the direction of the applied magnetic field. By harnessing the dynamic shape transformation, the magneto-elastomer can manipulate the flow direction and velocity in fluidic systems.

In magneto-mechanical metamaterials, shape transformation often significantly changes their area density and overall dimensions during magnetic actuation due to the internal deformations of the unit cells. Recently, Sim et al. (2023) presented a 2D magneto-mechanical bilayer metamaterial made of hard-magnetic soft materials that can maintain its overall area while tuning the acoustic/elastic bandgaps and wave propagations under external magnetic fields. As shown in Fig. 6(c), the bilayer unit cell is designed by overlaying two units with flipped magnetization distributions. The magnetization distribution is carefully designed such that only one layer can be actuated regardless of the direction of the applied magnetic field and thus, preserving its global area during reconfiguration. The flipped bilayer can exhibit four different modes by controlling the magnitude and direction of the applied magnetic field, including the initial, intermediate, top layer folded, and bottom layer folded modes. More importantly, each of the four modes has a constant global dimension but shows different acoustic/elastic bandgaps, as shown in Fig. 6(c). On the other hand, the actuated shape of magneto-mechanical metamaterials by magnetic control usually cannot be held once the applied magnetic field is removed. Recently, inspired by the reversible and shape-locking transformations in magnetic-SMP (Ze et al., 2020), Zou et al. (2023) presented an SMP lattices made of poly(lactic acid) (PLA) with permanent magnets embedded on the vertices, as shown in Fig. 6(d), which can transform into prescribed shapes and recover to its initial configuration under magnetic field and heating. By exploiting the reprogrammable transformation of the SMP lattice, they designed a series of magneto-thermomechanical metamaterials with multimodal deformation and shape locking capacities. Two examples are presented at the bottom of Fig. 6(d), which possess tunable Poisson's ratio and stiffness, respectively.

4.2. Snap-through instability enabled magneto-mechanical metamaterials

Another popular method to construct magneto-mechanical metamaterials is to harness the snap-through instabilities of bistable or multistable structures under magnetic actuation. Recently, Chen et al. (2021a) introduced a mechanical metamaterial consisting of an array of physical binary elements, which enables stable memory and on-demand reprogrammability of mechanical properties. As shown in Fig. 7(a), each binary element is a magnetic bistable elastic conical shell which can independently and reversibly switch between its two stable states, i.e., the ON and OFF states, under magnetic actuation. The two states exhibit distinct mechanical responses such as structural stiffness, yield strength, and stored strain energy (which can be extracted from the force-displacement curves). Specifically, the ON state is quite stiff, while the OFF state is relatively soft. The transition from the OFF state to the ON state leads to an increase in all three quantities by nearly an order of magnitude. By tessellating $n \times n$ binary elements into a square-lattice configuration, the obtained planar-array structure can exhibit n^2+1 different mechanical responses. Pal and Sitti (2023) presented a mechanical response programable metamaterial using bistable curved beams made of hard-magnetic soft materials, as shown in Fig. 7(b). By periodically linking multiple bistable beam elements in a lattice, the metamaterial system allows for the propagation of transition waves, where the transition distance, speed, and direction can be effectively controlled by the remotely applied magnetic field. Moreover, the metamaterial can be used to create mechanical logic gates for binary logical operations. Also, functionalities of the logic gate can be programmed by merely changing the external magnetic field. Zhang et al. (2023a) designed a magnetic field-induced asymmetric mechanical metamaterial with tunable local resonant bandgap, as shown in Fig. 7(c). The resonating cores are made of hard-magnetic soft materials which are connected to the elastomeric matrix by highly deformable curved beams. Under magnetic actuation, the induced magnetic body torque rotates the core and deforms the curved beam, and thus alters the natural frequency of the resonators. When the magnetic field is large enough, the magnetic torque triggers the snap-through of the curved beams and brings the metamaterial to a new stable configuration. By changing the applied magnetic induction, the local resonant bandgap can be tuned within a broadband low-frequency range.

In addition to bistable shells and beams, kirigami-inspired rotating squares are also employed to create bistable or multistable metamaterials by embedding permanent magnets into the squares (Slesarenko, 2020; Tipton et al., 2012; Yasuda et al., 2020). Recently, Korpas et al. (2021) integrated liquid crystal elastomers (LCEs) with such a kirigami system and designed a temperature-responsive multistable metamaterial. As shown in Fig. 7(d), the rotating squares with embedded magnets are connected by small hinges consisting of an LCE layer and a polydimethylsiloxane (PDMS) layer. When the temperature is changed, the LCE layer contracts and softens with respect to the PDMS layer, which causes the bilayer hinges to bend and the squares to rotate. Competition between the magnetic potential of the squares and the elastic energy of the hinges creates multiple stable states for the metamaterial. As the temperature increases from 25 °C to 80 °C, the initially monostable metamaterial first changes to tristable and then becomes bistable. By linking multiple individual units into chains to form a mechanical metamaterial, the metamaterial allows for the propagation of transition waves, and its propagation behavior can be tuned by

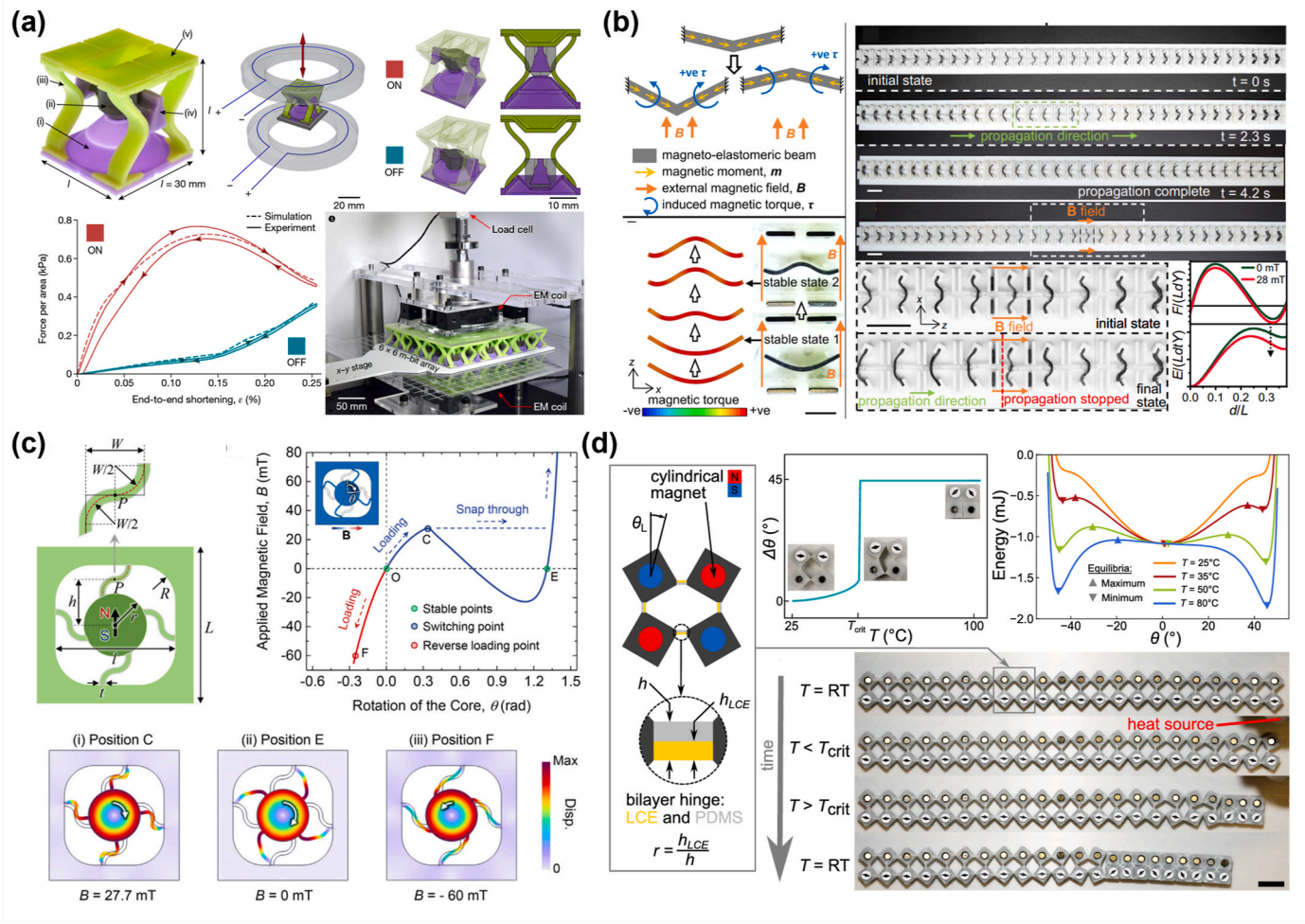

Fig. 7. Magneto-mechanical metamaterials enabled by snap-through instability. (a) Mechanical metamaterial consisting of bistable conical shells with magnetic caps. The caps are made of hard-magnetic soft materials, which can generate a torque to trigger the snapping of the shell under magnetic actuation. (b) Mechanical metamaterial consisting of bistable curved beams. The two segments of the curved beam have opposite magnetization directions. (c) Mechanical metamaterial consisting of resonating cores made of hard-magnetic soft materials. The cores are connected with an elastomeric matrix through highly deformable curved beams. (d) Multistable mechanical metamaterial consisting of rotating squares and LCE-PDMS bilayer hinges. The squares are embedded with permanent magnets. Fig. (a) is reproduced with permission from Chen et al. (2021a). Copyright 2021. The Authors, under exclusive license to Springer Nature Limited. Fig. (b) is adapted with permission from Pal and Sitti (2023). Copyright 2023. The Authors. Published by PNAS. Fig. (c) is reproduced with permission from Zhang et al. (2023a). Copyright 2023. The Authors. Published by Elsevier. Fig. (d) is reproduced with permission from Korpas et al. (2021). Copyright 2021 by American Chemical Society.

controlling its temperature. Moreover, Liang et al. (2022) presented a bistable elasto-magnetic metamaterial by embedding permanent magnets into a polymeric sheet with orthogonally aligned elliptical pores. The metamaterial can reversibly transition between an open phase (having pores between adjacent units) and a closed phase (no pores between adjacent units) under an external force. They showed that phase transition of the metamaterial not only alters its constitutive response but also significantly improves the energy release in dynamic recoil and mitigates the impact loading.

5. Design optimization of hard-magnetic soft materials

Although hard-magnetic soft materials have enabled diverse functional applications, most designs rely on experimental trial and error or intuition-based approaches, which may limit the design freedoms and application potentials of hard-magnetic soft materials. Recently, researchers have started to design hard-magnetic soft materials with predefined properties or deformations by employing optimization-based methods, such as machine learning (Ma et al., 2022; Lloyd et al., 2020; Yao et al., 2023), evolutionary algorithms (Lum et al., 2016; Wu et al., 2020a; Wang et al., 2021), topology optimization (Zhao and Zhang, 2022, 2023; Wang et al., 2023a), and gradient-based optimization (Wang et al., 2023b).

5.1. Machine learning-guided design

Machine learning techniques are a type of novel artificial intelligence that have emerged in recent years and have been widely used in various fields. They have also been recently employed in the design of hard-magnetic soft materials. Lloyd et al. (2020) proposed an inverse design method based on artificial neural network (ANN) for planar cantilever beams made of hard-magnetic soft materials with predefined deformations under magnetic actuation. The database for training the ANN was created by performing many finite element simulations. By using the trained ANN, the corresponding magnetization profile for a multi-segment cantilever beam to achieve predefined deformations under a uniform magnetic field can be found. Ma et al. (2022) presented a deep learning-guided inverse design framework for magneto-mechanical metamaterials with predefined global strains under magnetic actuation. In their work, a discrete artificial bee colony algorithm is adopted to optimize the magnetization distribution (including directions and magnitudes) for the target strains, in which a deep residual network is trained

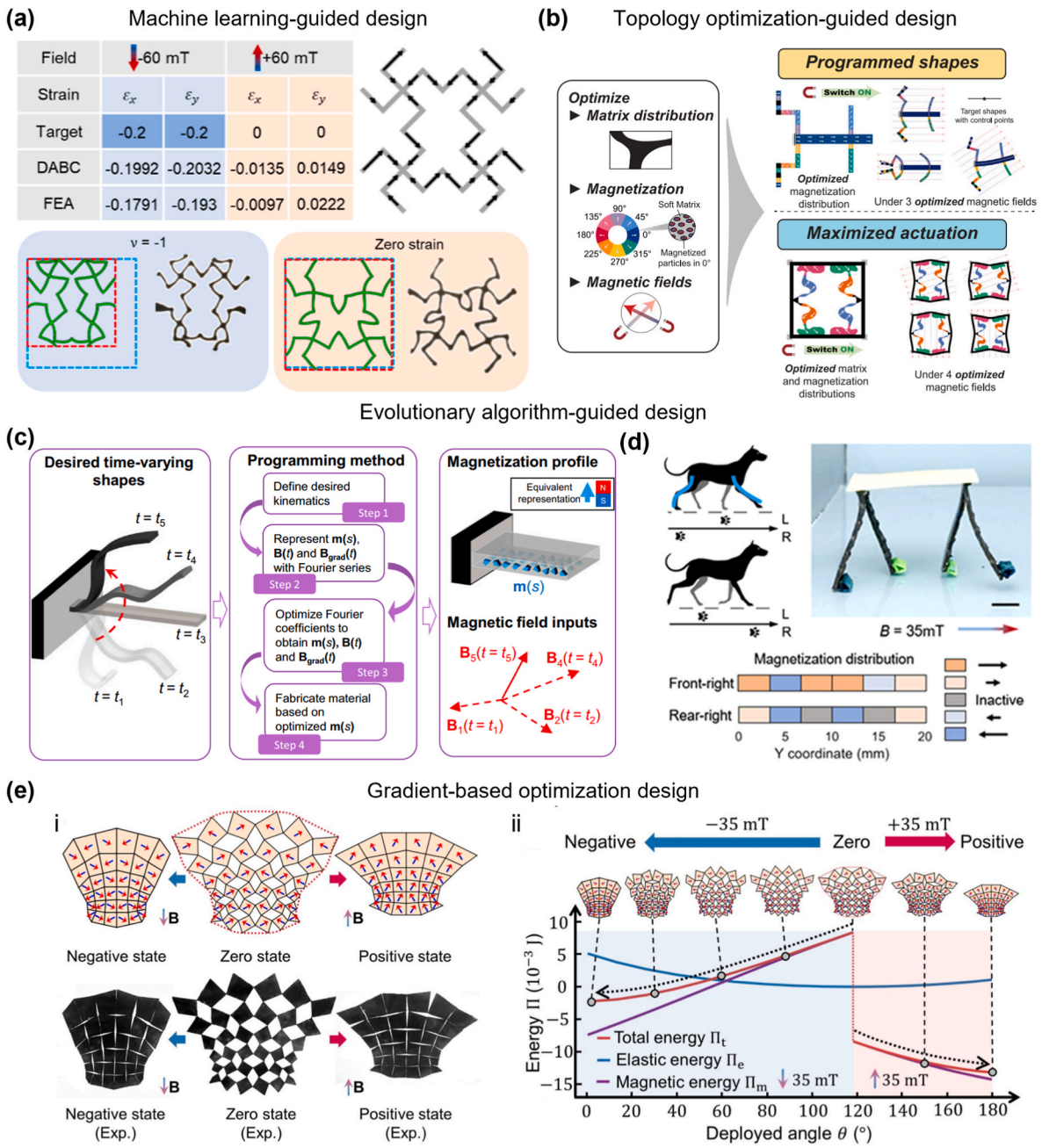

Fig. 8. Optimization design of hard-magnetic soft materials. (a) Machine leaning-guided design of a magneto-mechanical metamaterial with different target strains under opposite magnetic fields. (b) Topology optimization-guided design of shape-morphing structures with programable shapes and maximum actuation. (c) Optimization framework for a cantilever beam that can achieve target time-varying deformations. (d) Evolutionary algorithm-guided design of a soft robot that can mimic the walking motion of a dog. (e–i) Gradient-based optimization enabled inverse design of active kirigami that can achieve target shapes. (e-ii) Energy landscape of the active kirigami during shape morphing. Fig. (a) is adapted with permission from Ma et al. (2022). Copyright 2022 by American Chemical Society. Fig. (b) is reproduced with permission from Zhao and Zhang (2022). Copyright 2021 by Elsevier. Fig. (c) is reproduced with permission from Lum et al. (2016). Published by PNAS. Fig. (d) is reproduced with permission from Wu et al. (2020a). Copyright 2020. The Authors. Published by WILEY-VCH Verlag GmbH & Co. KGaA, Weinheim. Fig. (e) are reproduced with permission from Wang et al. (2023b). Copyright 2023. The Authors.

to replace the time-consuming finite element simulations to accelerate the optimization. The unit cell of the magneto-mechanical metamaterial to be optimized is shown in Fig. 8(a), which consists of 32 magnetic segments. For each segment, there are nine different possible magnetization distribution assignments. By using the established inverse design framework, magneto-mechanical metamaterials with optimized magnetization distributions that can achieve different target strains under opposite magnetic fields were designed, such as the demonstration shown in Fig. 8(a). The metamaterial has an equal target strain −0.2 in x- and y-directions under a negative magnetic field, while it exhibits zero strain under a positive magnetic field. Recently, Yao et al. (2023) developed an inverse design strategy based on deep reinforcement leaning algorithms to find desired magnetic fields to actuate strip-like magnetic soft robots. To achieve this, the authors presented a Cosserat rod model incorporating magnetic torques and dissipation forces which could simulate the dynamic behavior of strip-like magnetic soft robots. Then, the reinforcement learning framework was trained using the results produced by the model. The trained framework can provide the information of magnetic fields to achieve the movement of strip-like soft robots with different magnetizations.

5.2. Topology optimization-guided design

Topology optimization is another widely used tool for the optimization design of hard-magnetic soft materials. Recently, Zhao and Zhang (2022) established a 2D topology optimization framework for the inverse design of hard-magnetic soft materials by simultaneously optimizing topology, remanent magnetization distribution, and applied magnetic fields. The optimized structures can achieve multiple target functionalities under the optimized magnetic fields. For example, as shown in Fig. 8 (b), the frog-inspired swimming robot (top) with the optimized magnetization distribution can achieve three different target shapes, and the optimized magnetic-responsive unit cell (bottom) can achieve four adaptable actuation modes under their corresponding optimized magnetic fields. Later, Wang et al. (2023a) extended the topology optimization framework to achieve programmable 3D shape morphing of hard-magnetic soft materials under magnetic actuation. Also, topology optimization has been utilized to design magneto-active metamaterials with reprogrammable properties which exhibit one response under pure mechanical loading while featuring a distinct response under combined mechanical and magnetic stimuli (Zhao and Zhang, 2023).

5.3. Evolutionary algorithm-guided design

Apart from machine learning and topology optimization, evolutionary algorithms have also been used to guide the rational design of hard-magnetic soft materials with programmable deformations or functionalities. Lum et al. (2016) proposed a universal programming method that can produce the required magnetization profile and magnetic fields for hard-magnetic soft materials to achieve prescribed time-varying shapes, as shown in Fig. 8(c). The programming methodology is demonstrated with a cantilever beam made of NdFeB particles and soft silicone rubber, whose deformation behavior can be programmed by tuning the magnetization profile $\mathbf{m}$, magnetic field $\mathbf{B}$, and spatial gradient of the magnetic field $\nabla\mathbf{B}$ (see Eqs. (3.1) and (3.2) in Section 3). To achieve a target deflection, the authors first represented the three vectors with their corresponding 1D Fourier series, and then employed an optimization method to find the optimal values of those Fourier coefficients. Based on the proposed programming methodology, a jellyfish-like robot, a spermatozoid-like undulating swimmer, and an artificial cilium that achieve desired movements were designed. In addition, Wu et al. (2020a) integrated an evolutionary algorithm-guided design strategy with the voxel-encoding direct-ink-writing (DIW) printing method, which allows for programming the magnetization distribution of hard-magnetic soft materials to achieve prescribed functional deformation and dynamic motions. One such example the authors present is the biomimetic soft robot shown in Fig. 8(d), which can mimic the walking motion of a dog. Based on the hard-magnetic elastica model and the genetic algorithm, Wang et al. (2021) presented an optimization design framework capable of maximizing the workspaces of magnetic soft continuum robots by tuning the magnetization and the volume fraction of the magnetic particles.

5.4. Gradient-based optimization design

Additionally, based on a gradient-based optimization approach, Wang et al. (2023b) developed a differentiable inverse design framework for kirigami made of hard-magnetic soft materials. By optimizing the cuts and magnetization distributions, the active kirigami can achieve a wide range of target shapes and transition between different stable states under magnetic actuation. For example, as shown in Fig. 8(e-i), the optimized kirigami achieves a target shape in the zero state, while morphing into two different compact states (negative state and positive state) under magnetic fields with the same magnitude but opposite directions. Energy landscape during the shape morphing is depicted in Fig. 8(e-ii). It is seen that the active kirigami resides in the minimum energy state (i.e., stable state) in all three configurations.

6. Conclusions and outlook

In this paper, we reviewed recent works on the mechanics of hard-magnetic soft materials. Several existing constitutive models that can describe the coupled magneto-elastic deformation of hard-magnetic soft materials were first introduced. Then, mechanical response of structures made of hard-magnetic soft materials under mechanical and magnetic loading was discussed with emphasis placed on the large deformations and instabilities of hard-magnetic rods, beams, plates, and shells. Also, various magneto-mechanical metamaterials with tunable mechanical properties or behavior enabled by shape transformation and snap-through instability were presented. In addition, optimization-guided inverse design strategies of hard-magnetic soft materials based on machine learning, evolutionary algorithms, topology optimization, and gradient-based optimization were introduced. Despite the recent progress on the mechanics of hard-magnetic soft materials, there is still considerable work left in the field. Here, we provide our points on the future challenges and potential directions.

- Although various constitutive models for hard-magnetic soft materials have been developed, all of them are limited to hard-magnetic soft materials with inactive polymeric matrices. Recently, several works have embedded hard-magnetic particles into an active polymer matrix, such as shape memory polymers (Ze et al., 2020) and liquid crystal elastomers (Sun et al., 2023), to achieve more functionalities. Therefore, developing constitutive models for hard-magnetic soft materials with active polymeric matrices is a potential direction worthy of study.
- Most of the existing works on the mechanical response of structures fabricated from hard-magnetic soft materials focus on slender rods or beams, little attention has been paid to hard-magnetic plates and shells. Hard-magnetic plate and shell elements have also been used in engineering applications (Chen et al., 2021a; Hu et al., 2018; Kim et al., 2018), and understanding their mechanical behavior is beneficial in guiding designs in related applications.
- Mechanical response of hard-magnetic soft materials has been extensively studied, yet most studies are limited to hard-magnetic soft materials under uniform magnetic fields. In practical applications, hard-magnetic soft materials may be subjected to nonuniform or time-varying magnetic loading (Lum et al., 2016; Hu et al., 2018; Xia et al., 2022; Ze et al., 2020). Therefore, it is important to study the mechanical response (e.g., large deformation and instability) of hard-magnetic soft materials under nonuniform or dynamic magnetic fields.
- Hard-magnetic soft materials have shown great potential in the design of magneto-mechanical metamaterials with tunable properties, but most of the related works are based on experimental trial and error or intuition-based forward design processes. How to achieve the inverse design of magneto-mechanical metamaterials with prescribed properties to meet specific application requirements remains largely unexplored. Although there are some works that have achieved such design (Ma et al., 2022; Zhao and Zhang, 2023), a significant effort is still required. For example, how to design magneto-mechanical metamaterials with prescribed acoustic/elastic bandgaps and energy landscapes is still underexplored.

In summary, hard-magnetic soft materials have been demonstrated to be a promising candidate for the design of multifunctional intelligent devices or systems. We envision that the present review can help researchers better understand the mechanics of hard-magnetic soft materials, and thus achieve more functional applications.

Author statement

Lu Lu: Methodology, Visualization, Writing - original draft. **Jay Sim**: Writing - review & editing. **Ruike Renee Zhao**: Conceptualization,

Project administration, Funding acquisition, Supervision, Writing - review & editing.

Declaration of competing interest

The authors declare that they have no known competing financial interests or personal relationships that could have appeared to influence the work reported in this paper.

Data availability

No data was used for the research described in the article.

Acknowledgments

This work was supported by the National Science Foundation Career Award CMMI-2145601 and National Science Foundation Award CMMI-2142789.

References

Abbasi, A., Sano, T.G., Yan, D., Reis, P.M., 2023. Snap buckling of bistable beams under combined mechanical and magnetic loading. Philosophical Transactions of the Royal Society A 381, 20220029.
Alam, Z., Padmanabhan, S., Sharma, A.K., 2023. Magnetically tunable longitudinal wave band gaps in hard-magnetic soft laminates. Int. J. Mech. Sci. 249, 108262.
Alapan, Y., Karacakol, A.C., Guzelhan, S.N., Isik, I., Sitti, M., 2020. Reprogrammable shape morphing of magnetic soft machines. Sci. Adv. 6, eabc6414.
Arruda, E.M., Boyce, M.C., 1993. A three-dimensional constitutive model for the large stretch behavior of rubber elastic materials. J. Mech. Phys. Solid. 41 (2), 389–412.
Bertoldi, K., Vitelli, V., Christensen, J., Van Hecke, M., 2017. Flexible mechanical metamaterials. Nat. Rev. Mater. 2, 1–11.
Chen, L., Tan, K., Yang, S., Deng, Q., 2022a. Evoking the snap-through instability in hard-magnetic soft materials: rapid actuation and giant deformation. Int. J. Solid Struct. 246, 111607.
Chen, T., Pauly, M., Reis, P.M., 2021a. A reprogrammable mechanical metamaterial with stable memory. Nature 589, 386–390.
Chen, W., Wang, L., 2020. Theoretical modeling and exact solution for extreme bending deformation of hard-magnetic soft beams. J. Appl. Mech. 87, 041002.
Chen, W., Wang, L., Yan, Z., Luo, B., 2021b. Three-dimensional large-deformation model of hard-magnetic soft beams. Compos. Struct. 266, 113822.
Chen, W., Yan, Z., Wang, L., 2020. On mechanics of functionally graded hard-magnetic soft beams. Int. J. Eng. Sci. 157, 103391.
Chen, X., Ni, X., Zhu, B., Wang, B., Chen, B., 2022b. Simulation and optimization of magnetoelastic thin shells. ACM Trans. Graph. 41, 1–18.
Cui, J., Huang, T.-Y., Luo, Z., Testa, P., Gu, H., Chen, X.-Z., Nelson, B.J., Heyderman, L.J., 2019. Nanomagnetic encoding of shape-morphing micromachines. Nature 575, 164–168.
Dadgar-Rad, F., Hossain, M., 2023. A micropolar shell model for hard-magnetic soft materials. Int. J. Numer. Methods Eng. 124, 1798–1817.
Dehrouyeh-Semnani, A.M., 2021. On bifurcation behavior of hard magnetic soft cantilevers. Int. J. Non Lin. Mech. 134, 103746.
Deng, H., Sattari, K., Xie, Y., Liao, P., Yan, Z., Lin, J., 2020. Laser reprogramming magnetic anisotropy in soft composites for reconfigurable 3D shaping. Nat. Commun. 11, 6325.
Frenzel, T., Kadic, M., Wegener, M., 2017. Three-dimensional mechanical metamaterials with a twist. Science 358, 1072–1074.
Garcia-Gonzalez, D., 2019. Magneto-visco-hyperelasticity for hard-magnetic soft materials: theory and numerical applications. Smart Mater. Struct. 28 (8), 085020.
Garcia-Gonzalez, D., Hossain, M., 2021. Microstructural modelling of hard-magnetic soft materials: dipole–dipole interactions versus Zeeman effect. Extreme Mechanics Letters 48, 101382.
Green, M.S., Tobolsky, A.V., 1946. A new approach to the theory of relaxing polymeric media. J. Chem. Phys. 14, 80–92.
Gu, H., Boehler, Q., Ahmed, D., Nelson, B.J., 2019. Magnetic quadrupole assemblies with arbitrary shapes and magnetizations. Sci. Robot. 4, eaax8977.
Gu, H., Boehler, Q., Cui, H., Secchi, E., Savorana, G., De Marco, C., Gervasoni, C., Peyron, Q., Huang, T.Y., Pane, S., Hirt, A.M., Ahmed, D., Nelson, B.J., 2020. Magnetic cilia carpets with programmable metachronal waves. Nat. Commun. 11 (1), 2637.
Hu, W., Lum, G.Z., Mastrangeli, M., Sitti, M., 2018. Small-scale soft-bodied robot with multimodal locomotion. Nature 554, 81–85.
Huang, T.-Y., Gu, H., Nelson, B.J., 2022. Increasingly intelligent micromachines. Annual Review of Control, Robotics, and Autonomous Systems 5, 279–310.
Huang, W., Liu, M., Hsia, K.J., 2023. A discrete model for the geometrically nonlinear mechanics of hard-magnetic slender structures. Extreme Mechanics Letters 59, 101977.
Jiang, H., Gu, H., Nelson, B.J., Zhang, T., 2023. Numerical study of metachronal wave-modulated locomotion in magnetic cilia carpets. Advanced Intelligent Systems 5 (10), 2300212.
Kadapa, C., Hossain, M., 2022. A unified numerical approach for soft to hard magneto-viscoelastically coupled polymers. Mech. Mater. 166, 104207.
Kim, Y., Parada, G.A., Liu, S., Zhao, X., 2019. Ferromagnetic soft continuum robots. Sci. Robot. 4 (33), eaax7329.
Kim, Y., Yuk, H., Zhao, R., Chester, S.A., Zhao, X., 2018. Printing ferromagnetic domains for untethered fast-transforming soft materials. Nature 558, 274–279.
Korpas, L.M., Yin, R., Yasuda, H., Raney, J.R., 2021. Temperature-responsive multistable metamaterials. ACS Appl. Mater. Interfaces 13, 31163–31170.
Lakes, R., 1987. Foam structures with a negative Poisson's ratio. Science 235, 1038–1040.
Li, X., Yu, W., Liu, J., Zhu, X., Wang, H., Sun, X., Liu, J., Yuan, H., 2023. A mechanics model of hard-magnetic soft rod with deformable cross-section under three-dimensional large deformation. Int. J. Solid Struct. 279, 112344.
Liang, X., Fu, H., Crosby, A.J., 2022. Phase-transforming metamaterial with magnetic interactions. Proc. Natl. Acad. Sci. USA 119, e2118161119.
Linder, C., Tkachuk, M., Miehe, C., 2011. A micromechanically motivated diffusion-based transient network model and its incorporation into finite rubber viscoelasticity. J. Mech. Phys. Solid. 59, 2134–2156.
Liu, J., Yang, Y., Li, M., Xu, F., 2023. A meshfree model of hard-magnetic soft materials. Int. J. Mech. Sci. 258, 108566.
Lloyd, P., Hoshiar, A.K., da Veiga, T., Attanasio, A., Marahrens, N., Chandler, J.H., Valdastri, P., 2020. A learnt approach for the design of magnetically actuated shape forming soft tentacle robots. IEEE Rob. Autom. Lett. 5, 3937–3944.
Lum, G.Z., Ye, Z., Dong, X., Marvi, H., Erin, O., Hu, W., Sitti, M., 2016. Shape-programmable magnetic soft matter. Proc. Natl. Acad. Sci. USA 113, E6007–E6015.
Ma, C., Chang, Y., Wu, S., Zhao, R.R., 2022. Deep learning-accelerated designs of tunable magneto-mechanical metamaterials. ACS Appl. Mater. Interfaces 14, 33892–33902.
Ma, C., Wu, S., Ze, Q., Kuang, X., Zhang, R., Qi, H.J., Zhao, R., 2021. Magnetic multimaterial printing for multimodal shape transformation with tunable properties and shiftable mechanical behaviors. ACS Appl. Mater. Interfaces 13, 12639–12648.
Montgomery, S.M., Wu, S., Kuang, X., Armstrong, C.D., Zemelka, C., Ze, Q., Zhang, R., Zhao, R., Qi, H.J., 2021. Magneto-mechanical metamaterials with widely tunable mechanical properties and acoustic bandgaps. Adv. Funct. Mater. 31, 2005319.
Mooney, M., 1940. A theory of large elastic deformations. J. Appl. Phys. 11 (9), 582–590.
Mukherjee, D., Rambausek, M., Danas, K., 2021. An explicit dissipative model for isotropic hard magnetorheological elastomers. J. Mech. Phys. Solid. 151, 104361.
Narayanan, P., Pramanik, R., Arockiarajan, A., 2023. Micromechanics-based constitutive modeling of hard-magnetic soft materials. Mech. Mater. 184, 104722.
Novelino, L.S., Ze, Q., Wu, S., Paulino, G.H., Zhao, R., 2020. Untethered control of functional origami microrobots with distributed actuation. Proc. Natl. Acad. Sci. USA 117, 24096–24101.
Ogden, R.W., 1972. Large deformation isotropic elasticity–on the correlation of theory and experiment for incompressible rubberlike solids. Proceedings of the Royal Society of London. A. Mathematical and Physical Sciences 326 (1567), 565–584.
Pal, A., Sitti, M., 2023. Programmable mechanical devices through magnetically tunable bistable elements. Proc. Natl. Acad. Sci. USA 120, e2212489120.
Qi, Z., Zhou, M., Li, Y., Xia, Z., Huo, W., Huang, X., 2021. Reconfigurable flexible electronics driven by origami magnetic membranes. Advanced Materials Technologies 6, 2001124.
Rahmati, A.H., Jia, R., Tan, K., Liu, L., Zhao, X., Deng, Q., Sharma, P., 2023a. Giant magnetoelectricity in soft materials using hard magnetic soft materials. Materials Today Physics 31, 100969.
Rahmati, A.H., Jia, R., Tan, K., Zhao, X., Deng, Q., Liu, L., Sharma, P., 2023b. Theory of hard magnetic soft materials to create magnetoelectricity. J. Mech. Phys. Solid. 171, 105136.
Rajan, A., Arockiarajan, A., 2021. Bending of hard-magnetic soft beams: a finite elasticity approach with anticlastic bending. Eur. J. Mech. Solid. 90, 104374.
Rambausek, M., Mukherjee, D., Danas, K., 2022. A computational framework for magnetically hard and soft viscoelastic magnetorheological elastomers. Comput. Methods Appl. Mech. Eng. 391, 114500.
Ren, Z., Hu, W., Dong, X., Sitti, M., 2019. Multi-functional soft-bodied jellyfish-like swimming. Nat. Commun. 10, 2703.
Rivlin, R.S., 1948a. Large elastic deformations of isotropic materials. I. Fundamental concepts. Phil. Trans. Roy. Soc. Lond. Math. Phys. Sci. 240 (822), 459–508.
Rivlin, R.S., 1948b. Large elastic deformations of isotropic materials IV. Further developments of the general theory. Phil. Trans. Roy. Soc. Lond. Math. Phys. Sci. 241 (835), 379–397.
Sano, T.G., 2022. Reduced theory for hard magnetic rods with dipole–dipole interactions. J. Phys. Math. Theor. 55, 104002.
Sano, T.G., Pezzulla, M., Reis, P.M., 2022. A Kirchhoff-like theory for hard magnetic rods under geometrically nonlinear deformation in three dimensions. J. Mech. Phys. Solid. 160, 104739.
Saxena, K.K., Das, R., Calius, E.P., 2016. Three decades of auxetics research−materials with negative Poisson's ratio: a review. Adv. Eng. Mater. 18, 1847–1870.
Seong, M., Kim, C., Lee, A., 2023. Mechanical response of magneto-active elastic hemispherical shells. Int. J. Mech. Sci. 239, 107890.
Sim, J., Wu, S., Dai, J., Zhao, R.R., 2023. Magneto-mechanical bilayer metamaterial with global area-preserving density tunability for acoustic wave regulation. Adv. Mater. 35, 2303541.
Slesarenko, V., 2020. Planar mechanical metamaterials with embedded permanent magnets. Materials 13, 1313.
Stewart, E.M., Anand, L., 2023. Magneto-viscoelasticity of hard-magnetic soft-elastomers: application to modeling the dynamic snap-through behavior of a bistable arch. J. Mech. Phys. Solid. 179, 105366.

Sun, Y., Wang, L., Zhu, Z., Li, X., Sun, H., Zhao, Y., Peng, C., Liu, J., Zhang, S., Li, M., 2023. 3D-Printed ferromagnetic liquid crystal elastomer with programmed dual-anisotropy and multi-responsiveness. Adv. Mater., 2302824
Tan, K., Chen, L., Yang, S., Deng, Q., 2022. Dynamic snap-through instability and damped oscillation of a flat arch of hard magneto-active elastomers. Int. J. Mech. Sci. 230, 107523.
Tipton, C., Han, E., Mullin, T., 2012. Magneto-elastic buckling of a soft cellular solid. Soft Matter 8, 6880–6883.
Wang, C., Zhao, Z., Zhang, X.S., 2023a. Inverse design of magneto-active metasurfaces and robots: theory, computation, and experimental validation. Comput. Methods Appl. Mech. Eng. 413, 116065.
Wang, L., Chang, Y., Wu, S., Zhao, R.R., Chen, W., 2023b. Physics-aware Differentiable Design of Magnetically Actuated Kirigami for Shape Morphing arXiv preprint arXiv: 2308.05054.
Wang, L., Guo, C.F., Zhao, X., 2022. Magnetic soft continuum robots with contact forces. Extreme Mechanics Letters 51, 101604.
Wang, L., Kim, Y., Guo, C.F., Zhao, X., 2020. Hard-magnetic elastica. J. Mech. Phys. Solid. 142, 104045.
Wang, L., Zheng, D., Harker, P., Patel, A.B., Guo, C.F., Zhao, X., 2021. Evolutionary design of magnetic soft continuum robots. Proc. Natl. Acad. Sci. USA 118, e2021922118.
Wu, S., Eichenberger, J., Dai, J., Chang, Y., Ghalichechian, N., Zhao, R.R., 2022. Magnetically actuated reconfigurable metamaterials as conformal electromagnetic filters. Advanced Intelligent Systems 4, 2200106.
Wu, S., Hamel, C.M., Ze, Q., Yang, F., Qi, H.J., Zhao, R., 2020a. Evolutionary algorithm-guided voxel-encoding printing of functional hard-magnetic soft active materials. Advanced Intelligent Systems 2, 2000060.
Wu, S., Hu, W., Ze, Q., Sitti, M., Zhao, R., 2020b. Multifunctional magnetic soft composites: a review. Multifunctional Materials 3, 042003.
Wu, S., Ze, Q., Dai, J., Udipi, N., Paulino, G.H., Zhao, R., 2021. Stretchable origami robotic arm with omnidirectional bending and twisting. Proc. Natl. Acad. Sci. USA 118, e2110023118.
Wu, S., Ze, Q., Zhang, R., Hu, N., Cheng, Y., Yang, F., Zhao, R., 2019. Symmetry-breaking actuation mechanism for soft robotics and active metamaterials. ACS Appl. Mater. Interfaces 11 (44), 41649–41658.
Wu, Z., Zhang, J., Wei, S., Chen, D., 2023. Kirchhoff rod-based three-dimensional dynamical model and real-time simulation for medical-magnetic guidewires. Comput. Methods Progr. Biomed. 240, 107646.
Xia, N., Jin, D., Pan, C., Zhang, J., Yang, Z., Su, L., Zhao, J., Wang, L., Zhang, L., 2022. Dynamic morphological transformations in soft architected materials via buckling instability encoded heterogeneous magnetization. Nat. Commun. 13, 7514.
Xing, Z., Yong, H., 2023. Numerical study on the instabilities of hard-magnetic soft materials with viscoelastic effects. Mech. Mater. 179, 104602.
Xu, T., Zhang, J., Salehizadeh, M., Onaizah, O., Diller, E., 2019. Millimeter-scale flexible robots with programmable three-dimensional magnetization and motions. Sci. Robot. 4, eaav4494.
Yan, D., Aymon, B.F., Reis, P.M., 2023. A reduced-order, rotation-based model for thin hard-magnetic plates. J. Mech. Phys. Solid. 170, 105095.
Yan, D., Pezzulla, M., Cruveiller, L., Abbasi, A., Reis, P.M., 2021. Magneto-active elastic shells with tunable buckling strength. Nat. Commun. 12, 2831.
Yang, Y., Li, M., Xu, F., 2022. A 3D hard-magnetic rod model based on co-rotational formulations. Acta Mech. Sin. 38, 222085.
Yao, J., Cao, Q., Ju, Y., Sun, Y., Liu, R., Han, X., Li, L., 2023. Adaptive actuation of magnetic soft robots using deep reinforcement learning. Advanced Intelligent Systems 5 (2), 2200339.
Yasuda, H., Korpas, L., Raney, J., 2020. Transition waves and formation of domain walls in multistable mechanical metamaterials. Phys. Rev. Appl. 13, 054067.
Ye, H., Li, Y., Zhang, T., 2021. Magttice: a lattice model for hard-magnetic soft materials. Soft Matter 17, 3560–3568.
Yi, S., Wang, L., Chen, Z., Wang, J., Song, X., Liu, P., Zhang, Y., Luo, Q., Peng, L., Wu, Z., 2022. High-throughput fabrication of soft magneto-origami machines. Nat. Commun. 13, 4177.
Yu, X., Zhou, J., Liang, H., Jiang, Z., Wu, L., 2018. Mechanical metamaterials associated with stiffness, rigidity and compressibility: a brief review. Prog. Mater. Sci. 94, 114–173.
Ze, Q., Kuang, X., Wu, S., Wong, J., Montgomery, S.M., Zhang, R., Kovitz, J.M., Yang, F., Qi, H.J., Zhao, R., 2020. Magnetic shape memory polymers with integrated multifunctional shape manipulation. Adv. Mater. 32, 1906657.
Ze, Q., Wu, S., Dai, J., Leanza, S., Ikeda, G., Yang, P.C., Iaccarino, G., Zhao, R.R., 2022a. Spinning-enabled wireless amphibious origami millirobot. Nat. Commun. 13, 3118.
Ze, Q., Wu, S., Nishikawa, J., Dai, J., Sun, Y., Leanza, S., Zemelka, C., Novelino, L.S., Paulino, G.H., Zhao, R.R., 2022b. Soft robotic origami crawler. Sci. Adv. 8, eabm7834.
Zhang, H., Wu, J., Fang, D., Zhang, Y., 2021. Hierarchical mechanical metamaterials built with scalable tristable elements for ternary logic operation and amplitude modulation. Sci. Adv. 7, eabf1966.
Zhang, Q., Cherkasov, A.V., Arora, N., Hu, G., Rudykh, S., 2023a. Magnetic field-induced asymmetric mechanical metamaterials. Extreme Mechanics Letters 59, 101957.
Zhang, Q., Rudykh, S., 2022. Magneto-deformation and transverse elastic waves in hard-magnetic soft laminates. Mech. Mater. 169, 104325.
Zhang, R., Wu, S., Ze, Q., Zhao, R., 2020. Micromechanics study on actuation efficiency of hard-magnetic soft active materials. J. Appl. Mech. 87, 091008.
Zhang, Y., Ma, Y., Yu, J., Gao, H., 2023b. Non-contact actuated snap-through buckling of a pre-buckled bistable hard-magnetic elastica. Int. J. Solid Struct. 281, 112413.
Zhao, R., Kim, Y., Chester, S.A., Sharma, P., Zhao, X., 2019. Mechanics of hard-magnetic soft materials. J. Mech. Phys. Solid. 124, 244–263.
Zhao, Z., Zhang, X.S., 2022. Topology optimization of hard-magnetic soft materials. J. Mech. Phys. Solid. 158, 104628.
Zhao, Z., Zhang, X.S., 2023. Encoding reprogrammable properties into magneto-mechanical materials via topology optimization. npj Comput. Mater. 9, 57.
Zheng, X., Lee, H., Weisgraber, T.H., Shusteff, M., DeOtte, J., Duoss, E.B., Kuntz, J.D., Biener, M.M., Ge, Q., Jackson, J.A., 2014. Ultralight, ultrastiff mechanical metamaterials. Science 344, 1373–1377.
Zou, B., Liang, Z., Zhong, D., Cui, Z., Xiao, K., Shao, S., Ju, J., 2023. Magneto-thermomechanically reprogrammable mechanical metamaterials. Adv. Mater. 35, 2207349.